Atmos. Chem. Phys. Discuss., 15, 3063–3125, 2015
www.atmos-chem-phys-discuss.net/15/3063/2015/
doi:10.5194/acpd-15-3063-2015

Atmospheric Chemistry and Physics Discussions

Ozone and aerosols tropospheric concentrations variability analyzed using the ADRIMED measurements and the WRF-CHIMERE models

L. Menut[1], S. Mailler[1], G. Siour[2], B. Bessagnet[3], S. Turquety[1], G. Rea[1], R. Briant[1], M. Mallet[4], J. Sciare[5], and P. Formenti[2]

[1]Laboratoire de Météorologie Dynamique, UMR CNRS 8539, Ecole Polytechnique, Ecole Normale Supérieure, Université P. M. Curie, Ecole Nationale des Ponts et Chaussées, Palaiseau, France
[2]Laboratoire Inter-Universitaire des Systèmes Atmosphériques, UMR CNRS 7583, Université Paris Est Créteil et Université Paris Diderot, Institut Pierre Simon Laplace, Créteil, France
[3]Institut National de l'Environnement Industriel et des Risques, Verneuil en Halatte, 60550, Parc Technologique ALATA, France
[4]Laboratoire d'Aérologie, UMR CNRS 5560, Université P. Sabatier, Toulouse, France
[5]Laboratoire des Sciences du Climat et de l'Environnement, UMR CNRS 8212, CEA, Université Versailles St Quentin, Gif sur Yvette, France and The Cyprus Institute, Environment Energy and Water Research Center, Nicosia, Cyprus

Received: 15 January 2015 – Accepted: 16 January 2015 – Published: 2 February 2015

Correspondence to: L. Menut (menut@lmd.polytechnique.fr)

Published by Copernicus Publications on behalf of the European Geosciences Union.

ACPD
15, 3063–3125, 2015

Abstract

The ozone and aerosols concentrations variability is studied over the Euro-Mediterranean area during the months of June and July 2013 and in the framework of the ADRIMED project. A first analysis is performed using meteorological variables, ozone and aerosols concentrations using routine stations network, satellite and specific ADRIMED project airborne measurements. This analysis is complemented by modelling using the WRF and CHIMERE regional models. It is shown that this period was not highly polluted, with a moderate ozone production and several precipitation periods, scavenging the aerosols. In addition, no significant vegetation fires events were observed. The CHIMERE model simulating all kind of sources (anthropogenic, biogenic, mineral dust, vegetation fires) for numerous aerosols species, the aerosol speciation was quantified: during the whole period, the aerosols were mainly constituted by mineral dust, sea salt and sulphates close to the surface, and mainly mineral dust in the troposphere. Compared to AERONET size distribution, it is shown that the model underestimates the coarse mode near mineral dust sources and overestimates the fine mode in the Mediterranean area, even if the total mass of aerosols and the optical depth are correctly reproduced.

1 Introduction

The Euro-Mediterranean region is surrounded by many urbanized and agricultural lands in the north, and arid regions in the south. This leads to numerous different pollution sources with a majority of anthropogenic and biogenic sources in the north and mineral dust in the south. In addition, and mainly during summer, vegetation fires are often observed. As previously studied by Moulin et al. (1998); Middleton and Goudie (2001); Kubilay et al. (2003) and Israelevich et al. (2012), among others, the summer period is characterized by a south to north flow from Africa, transporting mineral dust in

ACPD
15, 3063–3125, 2015

the free troposphere, and a north to south flow transporting trace gases and particles of anthropogenic origin in the boundary layer, as summarized in Fig. 1.

In order to study the atmospheric composition over this region, the experimental part of the *"Aerosol Direct Radiative Impact on the regional climate in the MEDiterranean region"* (ADRIMED) project (Mallet, 2014) was conducted during the summer of 2013. ADRIMED is part of the international program ChArMEx (Dulac et al., 2013), aiming at assessing the present and future state of atmospheric chemistry in the Mediterranean area and its impact on regional climate, air quality, and marine ecosystems. This project completements several previous studies dedicated to the analysis of ozone and aerosols over the Mediterranean area.

Gerasopoulos et al. (2005) showed that ozone is controlled by production over the continent and may reach up to 60 ppb in the eastern Mediterranean marine boundary layer. Kalabokas et al. (2008) showed that the high concentrations observed are mainly driven by the anticyclonic meteorological conditions occuring during the summer. During the MINOS campaign (Lelieveld et al., 2002), conducted in altitude and over the same region, Roelofs et al. (2003) reported ozone concentrations of about 50 ppb, with peaks reaching 120 ppb. Lidar observations of ozone undertaken during the ESCOMPTE campaign (Cros et al., 2004) in Summer in the western part of the Mediterranean showed that highly concentrated plumes may be formed over a given country and be transported on several hundred of kilometers, before reaching ground levels (Colette et al., 2006).

Aerosols are also highly variable in space, time and composition. The latter depends on the relative contribution of various chemical species such as organic matter, sulphates, nitrates, ammonium, mineral dust and sea salt (Millan et al., 2005; Monks et al., 2009). Many experimental research programs were recently conducted to characterize the aerosols life cycle using surface measurements (Querol et al., 2009), airborne measurements (Dulac and Chazette, 2003), optical thicknesses deduced from sunphotometers (Kubilay et al., 2003), lidar measurements (including EARLINET) (Papayannis et al., 2008; Pappalardo et al., 2014) or satellite data (Barnaba and Gobbi,

ACPD
15, 3063–3125, 2015

2004). Remote-sensing surface measurements are also used to better quantify the dust optical properties and direct radiative forcing as in (Bergamo et al., 2008; Basart et al., 2009; Mallet et al., 2013; di Sarra et al., 2008). The integrated project EUCAARI (Kulmala et al., 2011), was conducted to better characterize the aerosols life cycle and composition in Europe, integrating many types of aerosols studies, from the nano to the global scales, with a large scientific community.

These measurements have been accompanied by significant developments in regional and global chemistry transport model (CTM). For example, ozone was simulated using the CHIMERE regional CTM during the ESCOMPTE campaign (Menut et al., 2005) and the summertime ozone maximum was analyzed using the TOMCAT global CTM Richards et al. (2013). Aerosols observations in the Mediterranean area often show large contributions from mineral dust, so that numerous studies were devoted to this species (Pérez et al., 2011; Nabat et al., 2012; Menut et al., 2013b; de la Paz et al., 2013). Their impact on climate via their radiative effect was recently analyzed with the models COSMO (Vogel et al., 2009), RegCM (Santese et al., 2010), SKYRON (Spyrou et al., 2013) and ALADIN-Climate (Nabat et al., 2014). Other important and still not well represented natural sources are now also included in CTMs. For example, sea salt were modelled in (Jiménez-Guerrero et al., 2011) and vegetation fires in (Turquety et al., 2014).

All these studies show that the ozone and aerosols are difficult to model in this region. Due to many different sources and their large variability, models have to include an accurate representation of all possible sources at the same time and of numerous chemical species, as well as the possibility to simulate the hourly concentrations.

The main purpose of this study is to better understand ozone and aerosols content in the lower troposphere over the Mediterranean area, using a combined analysis of atmospheric measurements and regional CTM simulations. The analyzed time period, from 1 June to 15 July 2013, is focused on the ADRIMED intensive campaign. The main questions addressed in this article are: *Was this period highly polluted in ozone and aerosols? What is the chemical composition of these aerosols? Is there a significant*

ACPD
15, 3063–3125, 2015

difference in this composition close to the surface and in altitude? What is the variability of the size distribution of these aerosols? The studied region encompasses North Africa and Europe, in order to take into account all possible ozone precursors and aerosols sources, and allow contributions from long-range transport.

To address these questions, this study follows three steps. First, measurements are analyzed to estimate when and where were the most important concentrations of ozone and aerosols observed in the Mediterranean area. Secondly, the ADRIMED period is simulated using the WRF-CHIMERE regional system. Comparisons between simulations and the available measurements allows an evaluation of the ability of the models to correctly reproduce the concentrations. Thirdly, having in mind the strengths and weaknesses of the modelling system, the ozone and aerosols composition is further analyzed. For ozone, the variability is quantified both at the surface and in altitude. For aerosols, the model provides additional informations such as composition and size distribution.

Section 2 presents the experimental framework of the ADRIMED campaign and the whole set of data (surface, soundings, aircraft measurements, satellite) used in this study. Section 3 presents the modelling system and the settings. Section 4 analyzes the meteorological situation using E-OBS data and the WRF model. Sections 5, 6 and 7 present ozone concentrations, aerosols optical depth and aerosols concentrations results, respectively. Sections 8 and 9 present aerosols speciation and size distribution. Conclusions and perspectives are presented in Sect. 10.

2 Observations

In this study, observations from both routine measurements and the ADRIMED intensive campaign are used.

In order to analyze meteorological parameters, the surface measurements provided by the E-OBS database are used. For ozone surface concentrations, observations from the EEA network are used. For aerosols, measurements from the AERONET photome-

ACPD
15, 3063–3125, 2015

ters are used, both for aerosol optical depth and size distribution. In order to have an overview of AOD over the whole region and the whole summer, satellite observations from the MODIS instrument are also used. The aircraft observations from the ADRIMED project are used to more finely analyze the vertical distribution of ozone. The location of the measurement sites used in this study is summarized in Table 1.

2.1 E-OBS meteorological measurements

In order to the modelled meteorology, comparisons with the daily average 2 m temperature and precipitation amount taken from the European Climate Gridded dataset (E-OBS) (Haylock et al., 2008) are undertaken. This dataset contains data collected from several thousands of meteorological stations throughout Europe and the Mediterranean area. These data are processed through a series of quality tests to remove errors and unrealistic values.

2.2 EEA chemical measurements

For regulatory pollutants, many measurements are routinely performed and well organized in homogeneous databases. The EEA (European Environmental Agency, (Guerreiro et al., 2013)) is responsible for the AirBase database used in this study. It contains surface concentrations measurements and information submitted by the participating countries throughout Europe (http://www.eea.europa.eu/). For this study, we focused on ozone and PM_{10}. In order to calculate scores and to study time series, a subset of data is used, including 8 "coastal background" and 9 "continental background" stations. Their location is displayed in Fig. 2 and details about their coordinates are provided in Table 1. They were chosen to be representative of various locations around the Western Mediterranean Sea: Spain, France and Italy, including the Baleares, Corsica and Lampedusa islands. These stations are all "background" stations, to ensure a correct representativity between the measured and the modelled values.

ACPD
15, 3063–3125, 2015

2.3 AERONET measurements

The AERONET (AErosol RObotic NETwork) photometers measurements (Holben et al., 2001), are used to characterize the observed Aerosol Optical Depth (AOD) and the volume Aerosol Size Distribution (ASD). The AOD data are recorded by numerous stations deployed around the world and hourly values are available. Several quality levels are proposed on the AERONET database (http://aeronet.gsfc.nasa.gov/). In this study, the level 2.0 is used for AOD and the level 1.5 for ASD, (Dubovik and King, 2000). The stations used in this study are listed in Table 1 and their location is displayed in Fig. 2.

2.4 ADRIMED measurements

The experimental part of the ADRIMED experiments includes surface measurements (at the super-sites of Cape Corsica and Lampedusa), remote sensing and airborne measurements, as presented in Mallet (2014). In this study, we focus on the surface measurements for temperature and precipitations. The airborne measurements are analyzed for ozone concentrations. These measurements were performed onboard the ATR-42 aircraft (operated by the SAFIRE CNRS, CNES and Météo-France joint laboratory). Nine flights were conducted during the studied period. The flight numbers, date and decimal hour, corresponding Julian day of flight are reported in Table 2. Trajectories are very different from one flight to another and are represented in Fig. 3 on a map and in Fig. 4 to see the vertical extension of the flights.

3 Modelling system

The modelling system is composed of several models: the WRF regional meteorological model, the CHIMERE CTM and additional individual models dedicated to emissions fluxes estimations. All these models are integrated in a modelling plat-form usable both

ACPD
15, 3063–3125, 2015

in analysis and forecast mode. The simulation was performed from 1 June to 15 July 2013.

3.1 WRF meteorological model

The meteorological variables are modelled with the non-hydrostatic WRF regional model in its version 3.5.1 (Skamarock et al., 2007). The global meteorological analyses from NCEP/GFS are hourly read by WRF using nudging techniques for the main atmospheric variables (pressure, temperature, humidity, wind). In order to preserve both large-scale circulations and small scale gradients and variability, the "spectral nudging" was chosen. This nudging was evaluated in regional models, as presented in Von Storch et al. (2000). In this study, the spectral nudging was selected to be applied for all wavelength greater than ≈ 2000 km (wavenumbers less than 3 in latitude and longitude, for wind, temperature and humidity and only above 850 hPa). This configuration allows the regional model to create its own structures within the boundary layer but makes sure it follow the large scale meteorological fields.

In this study, the model is used with a constant horizontal resolution of 60 km × 60 km and 28 vertical levels from the surface to 50 hPa, as displayed in Fig. 5. The Single Moment-5 class microphysics scheme is used, allowing for mixed phase processes and super cooled water Hong et al. (2004). The radiation scheme is RRTMG scheme with the MCICA method of random cloud overlap Mlawer et al. (1997). The surface layer scheme is based on Monin–Obukhov with Carslon–Boland viscous sub-layer. The surface physics is calculated using the Noah Land Surface Model scheme with four soil temperature and moisture layers Chen and Dudhia (2001). The planetary boundary layer physics is processed using the Yonsei University scheme Hong et al. (2006) and the cumulus parameterization uses the ensemble scheme of Grell and Devenyi (2002).

ACPD
15, 3063–3125, 2015

3.2 CHIMERE chemistry-transport model

CHIMERE is a CTM allowing the simulation of concentrations fields of gaseous and aerosols species at a regional scale. It is an off-line models, driven by pre-calculated meteorological fields. In this study, the version fully described in Menut et al. (2013a) is used. The simulations are performed over the same horizontal domain as the one defined for WRF. The 28 vertical levels of the WRF simulations are projected onto 20 levels from the surface up to 300 hPa.

The chemical evolution of gaseous species is calculated using the MELCHIOR2 scheme and that of aerosols using the scheme developed by Bessagnet et al. (2004). This module takes into account sulphate, nitrate, ammonium, primary organic matter (POM) and elemental carbon (EC), secondary organic aerosols (SOA), sea salt, dust and water. The aerosol size is represented using ten bins, from 40 to 40 µm, in diameter. The aerosol life cycle is completely represented with nucleation of sulphuric acid, coagulation, adsorption/desorption, wet and dry deposition and scavenging. This scavenging is represented by both coagulation with cloud droplets and precipitation. The formation of SOA is also taken into account.

The photolysis rates are explicitly calculated using the FastJX radiation module (version 7.0b), (Wild et al., 2000; Bian et al., 2002). The modelled AOD is calculated by FastJX for the 600 nm wavelength over the whole atmospheric column. A complete analysis of the improvement obtained in the model with this on-line calculation is fully described in a companion paper, Mailler (2014).

At the boundaries of the domain, climatologies from global model simulations are used. In this study, outputs from LMDz-INCA (Szopa et al., 2009) are used for all gaseous and aerosols species, except for mineral dust. For this species, simulations from the GOCART model are used (Ginoux et al., 2001).

The anthropogenic emissions are estimated using the same methodology as the one described in Menut et al. (2012) but with the HTAP (Hemispheric Transport of Air Pollution) annual totals as input data. These masses were prepared by the EDGAR

ACPD
15, 3063–3125, 2015

Team, using inventories based on MICS-Asia, EPA-US/Canada and TNO databases (http://edgar.jrc.ec.europa.eu/htap_v2). Biogenic emissions are calculated using the MEGAN emissions scheme (Guenther et al., 2006) which provides fluxes of isoprene and monoterpenes. In addition to this version, several processes were improved and added in the framework of this study. First, the mineral dust emissions are now calculated using new soil and surface databases, Menut et al. (2013b) and with a spatial extension of potentially emitting areas in Europe as described in Briant et al. (2014).

Emission fluxes produced by biomass burning are estimated using the new high resolution fire model presented in Turquety et al. (2014). Taking into account these fluxes is a major improvement in the CHIMERE model. Figure 6 presents the location of burned area during the summer of 2013, as detected by the MODIS satellite-based instrument (MCD64 product at 500 m resolution, processed as described in Turquety et al. (2014) and gridded onto the CHIMERE grid). The week number of first fire detection within each model grid cell ranges from 1 (the first week of June 2013) to 12 (the last week of September 2013). It shows that a majority of first fire event occured during the weeks 8 to 12, i.e. during September. These fires are mainly located in Portugal and Russia, and to a lesser extent, Greece. For each model grid cell, the number of fire events is presented (i.e. the number of area burned detections). For a large majority of diagnosed fires, this number is one, showing there were not a lot of fires during the summer of 2013.

4 Analysis of meteorology

This WRF model configuration was already compared to measurements for the same kind of domain, resolution and use with the CHIMERE model in Mailler et al. (2013); Menut et al. (2013b) and Menut et al. (2013c) for example. It was shown that the model is able to accurately reproduce the main meteorological variables over the Euro-Mediterranean area and to provide realistic enough fields for chemistry-transport modelling. However, since the model results also depend on the studied period, the 2 m

ACPD
15, 3063–3125, 2015

temperature and the precipitation amount are here compared to the available data of E-OBS.

4.1 Daily maps

A comparison of 2 m temperature, $T_{2\,m}$, (K) and precipitation amount, Pr, (mm day^{-1}) is presented in Fig. 7. Three days are selected as representative of the studied period: 16, 20 and 24 June 2013. For each day and for the WRF results, the hourly 2 m temperature is averaged over the day and the hourly precipitation amount (mm h^{-1}) is cumulated to have mm day^{-1}. For the E-OBS observations, values are available over land only. For the WRF model, 2 m temperature and precipitation amount are available over the whole model domain, even if this domain is limited to a maximum latitude of 55° N.

For the 2 m temperature, we note that the observed and modelled values are similar. For example, and over Germany, a maximum of $T_{2\,m}$ is observed during the 20 June, also well modelled by WRF. For Pr, the main structures and the relative amount are also well modelled. For the 16 June, the E-OBS data diagnosed precipitations in the western part of UK, France and Spain. WRF is able to modelled this pattern and shows a large precipitation system over the Atlantic sea. This system is advected to the eastern part of Europe and the WRF model is able to reproduce this advection speed as well as the accumulated precipitation values. These comparisons show the model is able to reproduce the main synoptic scale absolute values and variability observed during this period.

4.2 Daily time series

From the E-OBS data daily maps, time series are extracted for some sites in Europe, as listed in Table 1. From 1 June to 15 July, for the grid cell corresponding to the site location, daily averages of the WRF model hourly results are computed for the 2 m temperature, and values are cumulated for precipitation. These comparisons are displayed in Fig. 8 and statistical scores are presented in Table 3.

ACPD
15, 3063–3125, 2015

For $T_{2\,m}$, the scores show that the correlation is high, ranging from 0.87 and 0.99. However, a non negligible bias is calculated, ranging between −4.1 and 0.87 K, showing the model mainly underestimates the E-OBS gridded values. This bias can not be attributed to a problem of measurements vs. model representativity, the E-OBS values being regridded with a 0.25° × 0.25° resolution and the model having a 60 km × 60 km horizontal resolution. This bias is more probably due to the boundary layer or microphysics schemes used with WRF in this study. The model is able to reproduce the main variability observed during the whole period: low temperatures observed in the first days of June, corresponding to precipitation events, then a warmest period, with temperatures increasing from ≈ 290 to ≈ 295 K in the 14 to 17 June. A second large precipitation event is observed from the 18 to 25 June (except in Bastia) leading to a slight cooling. After the 25 June, precipitations are observed and modelled, but they are more moderate and the temperature increases from ≈ 290 to ≈ 295 K until the end of the studied period, 14 July 2013.

These time series also show that the daily precipitation amount Pr has the same order of magnitude in the observations and the model simulations: when a precipitation event is observed over one site and during one day, the meteorological model is able to capture this event. If the absolute values do not match exactly, the main effect for atmospheric composition is present: wet scavenging would occur at the right place and right time to remove particles in the atmosphere. In order to quantify the ability of the model to reproduce these precipitations events in terms of aerosols scavenging, the correlation coefficient is not the adaptated metric. We introduce the hit rate score: for a threshold arbitrarily chosen as $Pr_T = 0.1\,mm\,day^{-1}$ (i.e. there is precipitation for this day and this site), the event is considered as true if $Pr > Pr_T$. If this condition is reached for the observations and the model, a counter increments the "a" value. If the condition is reached for the observations and not the model, a counter increments the "c" value. The Hit Rate, HR, is defined as:

$$HR = \frac{a}{a + c} \quad (1)$$

ACPD
15, 3063–3125, 2015

The target value for the Hit Rate is 1, meaning that the model was able to catch all the observed events. Results are presented in Table 4. The number of events is also displayed since precipitations did not occur every day. The number of days under a precipitation event is between 1 to 19 for a total of 41 studied days. The HR ranges from 0.64 to 1, showing that the model correctly reproduces this variable. One also notes that the mean bias is often negative, showing that the modelled precipitations are lower than what was observed.

5 Analysis of ozone concentrations

The first comparisons between measured and modelled atmospheric composition are undertaken for the analysis of ozone concentrations near the surface and in altitude. Ozone reflects the amount of photo-oxidant pollution, especially during summertime periods. Two kinds of data are used in this section: (i) the routine surface measurements of the AirBase background stations and (ii) the airborne measurements done for ADRIMED with the ATR aircraft. The AirBase measurements are regular in time (hourly), and are used to quantify if the model is able to simulate both the background values and the peaks during high pollution events. However, being only at the surface, these measurements are not dedicated to provide an information on the model behaviour in the whole troposphere. Thus, they do not allow an interpretation on the ozone long range transport. The ATR measurements are then complementary, providing vertical ozone profiles at a given time. However, unlike surface observations, they are very specific and do not reflect the overall situation of atmospheric pollution over the whole Mediterranean area.

5.1 Ozone surface concentrations maps

Simulated surface ozone concentrations are displayed in Fig. 9. The three maps are selected to present values for the same days as for the meteorological variables in

ACPD
15, 3063–3125, 2015

Fig. 7. For the 16 June 2013 and over the Mediterranean sea, ozone values vary a lot, between 30 and 70 $\mu g\,m^{-3}$, with several plumes having a spatial extent of a few tens of kilometers only. The most important surface concentrations are modelled in the south eastern part of the domain, over Saudi Arabia. Surface concentrations are much higher on 20 June 2013 over Europe. This corresponds to the highest $T_{2\,m}$ values, enhancing the photochemical processes over anthropogenic sources such as Belgium and the Netherlands. Over Great Britain and France, values are low and this corresponds to cloudiness associated with the observed and modelled precipitations. On 24 June, ozone concentrations are low (less than 40 $\mu g\,m^{-3}$) over the whole Europe. This corresponds to the advection of this precipitation event from west to east. Finally, these maps show that ozone concentrations were moderated during this ADRIMED period, except over Saudi Arabia.

5.2 Ozone surface concentrations time series

To better understand the daily variability observed on the maps, scores are calculated for daily maximum and daily mean averaged values. Results are presented in Table 5 (daily maximum) and Table 6 (daily mean). The corresponding time series are presented in Fig. 10 for the daily maximum values. Results are split as a function of the AirBase surface station type (coastal or continental).

The scores reported in Table 5 show the ability of the model to capture extreme events. Depending on the location, the model simulates lower or higher maximum daily values, compared to the measurements. But for all stations, the differences between the two is never more than 20 $\mu g\,m^{-3}$. The correlations are also very dispersed, with values ranging from 0.15 (Malaga) to 0.71 (Agen). One can expect to have better correlations over the continent than over the sea due to the formation processes of ozone. This is not always the case, showing the difficulty of the model to estimate daily peaks over this complex region.

The scores in Table 6 are complementary and present results for hourly values. In this case, the complete diurnal cycle of ozone formation is taken into account. The

ACPD
15, 3063–3125, 2015

scores are often better than for the daily peaks, with values up to 0.81 (Cordoba). The low correlation results are obtained for Ajaccio and Malaga (0.40), Bastia (0.29) and Gap (0.36), as already diagnosed with the daily peaks. This denotes a general unability of the model to represent ozone formation and transport over these areas. For these three sites, the problem is probably related to the low model resolution, these three sites being in mountainous or insular areas, the subgrid scale variability of ozone remains difficult to model.

Time series of measured and modelled ozone daily maximum are displayed in Fig. 10. For the coastal stations, Ajaccio, Bastia and Zorita, the measured values show flatter time series than the modelled ones, explaining low correlations obtained in Ajaccio and Bastia. When the model overestimates the concentrations in Ajaccio, it underestimates the concentrations in Bastia, even if the locations are close and located in the Corsica Island. From a model point of view, this consists in two close (but not neighboring) grid cells. These high differences may be explained by zooming on Corsica as displayed in Fig. 11: ozone surface concentrations (in ppb) are shown for the 17 June 2013, 12:00 UTC, as an example. For this day, and more generally for the whole ADRIMED period, surface ozone concentrations are very variable and composed of very dense and isolated plumes. This explains the large variability of scores when comparing point by point model and surface measurements, even if the horizontal resolution is coarse.

The scores are better for continental stations as Champforgeuil and Agen. The model is able to capture the day to day variability, with highest values recorded for the 16–17 June and 6–10 July. This corresponds to well established polluted periods, but the maximum values of 140 $\mu g\,m^{-3}$ are far from high pollution events.

5.3 Ozone and meteorological vertical profiles during the ATR flights

The ozone concentrations measured during the ATR flights are averaged from 1 Hz to a 5mn time step. The number of averaged data is reported in Table 2. The simulated concentrations corresponding to the location of the measurement are interpolated in

ACPD
15, 3063–3125, 2015

time (between the two modelled hourly outputs), vertically (between the two model vertical levels) and horizontally (using a bilinear interpolation). The comparison between the modelled and measured ozone concentrations is presented in Fig. 12. The corresponding altitude, temperature (in °C) and mean wind speed (in $m s^{-1}$) are also presented, using the same abscissa axis.

Each flight lasts between two and three hours. In the altitude panels, we can see that the aircraft made several iso-altitude measurements, mainly at 4000 and 6000 m. For meteorological data, the temperature is always very well simulated by the WRF model. The differences between model and measurements are very weak, except, for example, for flights 30 and 31 where the temperature is slightly more underestimated by the model in altitude than close to the surface. The wind is variable and there are differences between simulated values and measurements, mostly in terms of variability, but the absolute values are correctly estimated.

Ozone is always over-estimated by the model, especially in altitude. This is probably a direct effect of boundary conditions that may be too strong for this period. The boundary chemical fields are derived from a global climate model and the summer of 2013 was moderated in terms of pollution: the climatology may thus induce a positive bias in the model. These flights within the marine boundary layer are a very good opportunity to evaluate ozone concentrations over the maritime surfaces. These concentrations are usually very high in models due to a lack of deposition. For measurements near the surface, the model is mostly closer to the measurements. Two peaks are simulated during flights 29 and 33 but are not measured: these modelled high ozone values correspond to local ozone plumes as presented in Fig. 9. However, the ozone peak close to the surface for the flight 30 is well captured.

6 Analysis of Aerosols Optical Depth

The Aerosols Optical Depth (AOD) reflects the extinction of radiation by aerosols along the whole atmospheric column. This quantity being well and often measured, the com-

ACPD
15, 3063–3125, 2015

parison between model and measurements is widely used to estimate the models' ability to reproduce aerosol plumes. However, comparisons of AOD have limitations. Being vertically integrated, there is no information on the vertical structure of the aerosol plume. In addition, AOD is estimated for a specific wavelength, not always representative of the complete size distributions of all aerosols. In this study, the CHIMERE outputs AOD are calculated at 600 nm, due to the fastJ algorithm used in the model.

6.1 Comparisons between MODIS and CHIMERE

The goal of this paper being to evaluate the ability of a model to estimate hourly pollutants concentrations in the boundary layer and the lower troposphere, the satellite measurements are here only used to first check if the main AOD patterns are well retrieved. The measured AOD at 550 nm is extracted from the MODIS satellite data over the period from 6 June to 15 July 2013. Observations are interpolated on the model grid and comparisons are done for collocated data in space and time, as displayed in Fig. 13. The MODIS map includes the AOD retrieved over ocean and over land, proposed on the NASA Giovanni database. MODIS AOD products have been used for many years to study the amount and origin of aerosols in the Mediterranean troposphere. Barnaba and Gobbi (2004) used these data to split relative contributions of aerosols on AOD. They showed that for the same particle size, its origin (maritime, continental or desert dust) may induce an AOD variability of one order of magnitude. More recently, Levy et al. (2010) evaluated the MODIS AOD product over land, by comparison to AERONET sunphotometer data. They showed that there is a high correlation (R = 0.9) between the two AOD products, with a mean bias of ±0.05.

The AOD data are time averaged over the period from 6 June to 15 July 2013 in order to have the maximum of available informations on the map. Figure 13 shows that, in average for all the considered period, CHIMERE reproduces realistically the main features of the AOD over the considered region, with average values above unity for the Sahelian band and the Arabian peninsula. However, CHIMERE misses high AOD values on the eastern side of the Caspian Sea as well as over the northern part

ACPD
15, 3063–3125, 2015

of the Atlantic. For the first area, the underestimation of the AOD by CHIMERE may be related to missing dust emissions, while for the northern Atlantic, the high AOD values in MODIS are related to an average computed from very few data points, possibly during an event of transport of a polluted plume (e.g. biomass burning or mineral dust) from outside of the simulation domain that is not present in the global climatologies used at the boundaries.

6.2 Comparisons between AERONET and CHIMERE

Comparisons between modelled and measured AOD are also done using the AERONET data (level 2) (Holben et al., 2001). Time series are presented in Fig. 14. While the station of Banizoumbou is located close to the mineral dust sources, the stations of Capo Verde and Dakar are directly under the plume. This explains that over the whole period, AOD values are high, ranging from 0.4 to 2. The day to day variability is also important and these time series show that the highest AOD values are observed during the period from 5 to 15 June. A second period with high values is between the 27 and 30 June, with values up to AOD = 1. The model is able to retrieve the observed day to day variability, even if, on average, modelled values are greater than observed ones for stations far away from the main Saharan dust sources.

Time series are also presented for the stations of Lampedusa, Forth Crete and Izana. This set of stations is representative of small islands (for Lampedusa and Izana) and remote locations (Forth Crete). The measured AOD values are always lower than 0.5. This clearly shows that, during the whole period, no intense aerosol plume was observed over the Mediterranean sea. The comparison results are not as good as for the African stations and the model tends to overestimate the AOD over the Mediterranean area. This overestimation may be due to several factors that can not be diagnosed only with the AOD, this quantity being an integrated budget of many possible contributions. This may be an overestimation of surface mineral dust emissions, a shift in the aerosols size distribution, or an underestimation of modelled dry deposition velocities. However,

ACPD
15, 3063–3125, 2015

considering all these potential problems, the AOD is satisfactorily modelled compared to the AERONET measurements.

Table 7 corresponds to statistical scores calculated over these AERONET stations. The number of observations is very variable from one station to another: if the Izana station has 516 measurements, Forth Crete has only 108. These differences are certainly due to the cloud screening algorithm applied on the raw sunphotometer data to ensure that provided AOD are only due to aerosols. The correlation is variable from one site to another with values ranging from 0.20 (Ilorin) to 0.77 (Izana) and 0.79 (Lampedusa). The RMSE is very large, of the order of magnitude of the AOD value, showing important discrepancies between model and measurements. The bias shows that the model underestimates AOD close to the sources and tends, contrarily, to overestimates AOD for remote sites such as Izana and Lampedusa.

7 Analysis of PM_{10} surface concentrations

For the understanding of the aerosols life cycle, the analysis of PM_{10} surface concentrations is complementary to the analysis of AOD. Comparisons are here presented between surface AirBase measurements and, for the corresponding location in the model domain, PM_{10} concentrations at the model's first vertical level.

7.1 Statistical comparisons between model and observations

Table 8 presents scores for this comparison. The values are daily averaged and are expressed in $\mu g\,m^{-3}$. The number of values compared is very variable and mostly between 700 and 1000, corresponding to hourly data over the whole period. Italian stations are different and measurements are only daily, leading to a lower number of raw observations. At the end, 33 to 41 daily averaged values are available. The observed values ranged from 7.9 (baceno) to 32.5 (Malaga) $\mu g\,m^{-3}$. For the model, the values ranged from 12.6 (Baceno) to 30.1 (Malaga) $\mu g\,m^{-3}$. If the variability from site to site

ACPD
15, 3063–3125, 2015

is correctly reproduced, the results showed that the model may underestimate or overestimate the concentrations, depending on the site. There is no obvious link between the location of the site and the sign of the difference: the bias may be positive or negative for sites in the same region. Depending on the station, the correlation ranges from very low (−0.02 for Cartagena and −0.04 for Agen, for example) to moderate (0.66 in Chitignano, 0.68 in Hyeres, 0.68 in Vercelli). For 11 stations (on a total of 17), the bias remains lower than $\pm 4\,\mu g\,m^{-3}$.

7.2 Surface concentrations time series

The measured and modelled daily averaged surface PM_{10} concentrations are presented in Fig. 15 as time series. On average, the background concentrations are well simulated for all sites. However, some discrepancies appear when some peaks are modelled but not measured, as for example at Zorita, Malaga and Agen. The lower bias on the AOD suggests that the whole column is correct, but that the surface concentrations are too large. This can be, partially, a problem of too important vertical dffusion, often diagnosed in deterministic Eulerian models (Vuolo et al., 2009). Another possibility is to have too important local emissions. A way to better understand this overestimation is to analyze the aerosols composition, as presented in the next section.

8 The modelled aerosols speciation

One goal of this paper is to calculate and discuss the chemical speciation of the aerosols. In the previous sections, the aerosols behaviour was analyzed in terms of AOD and surface PM_{10}. In this section, aerosol composition is analyzed and results are presented in terms of time series of surface concentrations and vertical profiles of concentrations.

ACPD
15, 3063–3125, 2015

8.1 Time series

For each site, the modelled aerosols composition is presented as surface time series in Fig. 16. The concentrations are shown for the whole aerosols size distribution, i.e. for a mean mass median diameter D_p from 0.04 to 40 µm. This is thus logical to have surface concentrations higher than the ones presented for the PM_{10} time series. All presented species correspond to CHIMERE model species with the secondary species families (such as SOA), the mineral dust (DUST) and the primarily emitted species (such as POM, EC and the rest of anthropogenic dust called PPM here). The complete explanations about these species are provided in Menut et al. (2013a). For all time series, the most important contribution comes from mineral dust, with, at least, 50 % of the total mass. This mineral dust part is also responsible of the large peaks observed on the PM_{10} concentrations. The second most important contribution corresponds to sea salts, specifically for locations corresponding to islands or for coastal sites such as Lampedusa and Cape Corsica. For "continental background" stations such as Champforgeuil and Agen, the concentrations are lower than for other stations and the relative part of sea salt becomes logically negligible. For days when there is no peak of dust and sea salt, sulphate concentrations dominate the aerosol composition. However, surface concentrations of mineral dust remain important for these stations suggesting that modelled local emissions are too large. The last most important contribution is for sulphates with large concentrations modelled in Lampedusa and Malaga, among others. Finally, the relative contributions of POM and EC are very low in the total, showing in particular that this period was not influenced by large vegetation fires events.

8.2 Relative contribution of chemical species

The time series presented in the previous section showed the large temporal variability of the surface concentrations as well as the large variability of the aerosol chemical composition. In order to quantify these relative contributions site by site, the relative amount of each chemical species is estimated as a percentage of the total concentra-

ACPD
15, 3063–3125, 2015

tion. The calculation is done by cumulating the hourly concentrations over the whole studied period and species per species. The results are presented in Table 9. For each site, the value of the most abundant species is bolded.

For 13 stations (out of a total of 17 stations), the most important species is mineral dust, with values ranging from 25.01 % (Champforgeuil) to 64.48 % (Cordoba). In general, the sites where mineral dust dominates correspond to the western part of the Mediterranean: Zorita, Cartagena, Malaga, Aranjuez, Cordoba (all these sites being in Spain).

The second most important contribution is sulphates: this is the most important component for the aerosols at sites Cape Corsica (28.39 %), Ajaccio (22.79 %), Bastia (28.05 %) and Schivenoglia (24.73 %). The first three sites are in Corsica and the last one in the North of Italy. For the sites in Corsica, these large amounts of sulphates are due to shipping emissions or the vicinity of the Fos-Berre industrial area in the South of France, when Schivenoglia is close to industries.

The third most important contribution is sea salt. For sites such as Lampedusa, Cartagena, Malaga, this contribution is close to the sulphate contribution values. All these sites correspond to island or coastal sites, and are thus more exposed to sea salt emissions. For all continental sites, the sea salt contribution is low, between 2 % (Baceno) and 12.76 % (Agen). Finally, only one site have a major contribution very different of the others: in Hyeres, the most important chemical species POM (Particulate Organic Matter) and this has to be linked to the vicinity of the Fos-Berre area, with organic carbon emissions.

8.3 Vertical profiles

In order to link the information of surface concentrations, aerosols composition and vertical structure, Figure 17 presents vertical profiles for the same stations as in Fig. 16 and for the 21 June 2013 at 12:00 UTC. Abscissa scales on the Figure are different in order to clearly see all profiles. The largest concentrations are modelled in Lampedusa, with a maximum of 280 $\mu g\,m^{-3}$ at 4000 m AGL. This maximum is due to the long range

ACPD
15, 3063–3125, 2015

transport of mineral dust from Africa. A peak of mineral dust in altitude is also modelled in Cape Corsica and Champforgeuil. In Cape Corsica, the maximum value is 30 $\mu g\,m^{-3}$ at 2500 m AGL, with a contribution of 16 $\mu g\,m^{-3}$ from mineral dust. In Champforgeuil, a mineral dust peak is modelled at 2000 m AGL with 12 $\mu g\,m^{-3}$. In this case, the peak is at 1000 m and mainly due to non negligible concentrations of sea salt, sulphates, nitrate and ammonium: mineral dust represents 6 $\mu g\,m^{-3}$ for a maximum value of 19 $\mu g\,m^{-3}$ at 1000 m AGL.

For Zorita, Malaga and Agen, the maximum concentrations are located close to the surface. They are lower than when mineral dust plumes are modelled, with maximum from 12 to 40 $\mu g\,m^{-3}$. The aerosols speciation varies for each site, as described in Table 9. Finally, for all these profiles, the mineral dust contribution corresponds to the main part of the aerosol composition in altitude, with important contributions of sulphates, from the surface up to 4000 m.

9 Aerosols size distributions

The understanding of aerosols concentrations after emissions, transport and chemistry is very sensitive to their size distribution. The size distribution is both difficult to measure and to model. Firstly, the size distribution varies with the emission process. After emission, this distribution will change over time as a function of settling and dry deposition. This section is dedicated to better understand the variability of the aerosols size distribution.

9.1 Observed and modelled aerosols size distributions

Observations from the AERONET inversion algorithm results (Dubovik and King, 2000) are used. For each AERONET station, the inversion algorithm provides volume particle size distribution for 15 bins, logarithmically distributed for radius between 0.05 to 15 µm. In CHIMERE, the aerosols size distribution is defined during the emissions

ACPD
15, 3063–3125, 2015

fluxes calculations and is different for each species (following the recommendation of the emissions inventories, as described in Menut et al. (2013a)). For all aerosols (except mineral dust), the distribution is fixed at the emission and then may only vary with heterogeneous chemistry and deposition. For mineral dust, the size distribution may vary at emission, depending on the wind speed and following the dust production model of Alfaro and Gomes (2001). In order to directly compare observations and model results, the modelled column aerosol volume size distribution is calculated for each model bin as in Péré et al. (2010):

$$\frac{\mathrm{d}V}{\mathrm{d}\,\log(D_\mathrm{p})} = \sum_{k=1}^{k=\mathrm{nlevels}} \frac{\left(\sum_{c=1}^{c=\mathrm{naero}} \frac{m_\mathrm{c}}{\rho_\mathrm{c}}\right) \times \Delta z_k}{\log(D_{\mathrm{p,max}}) - \log(D_{\mathrm{p,min}})} \tag{2}$$

where: m_c is the mass concentration (the mass of particles in a volume of air, in $\mu\mathrm{g\,m^{-3}}$) for the naero modelled aerosols. ρ_c is the particle density (also in $\mu\mathrm{g\,m^{-3}}$, the mass of the particle in its own volume). In this model version, all aerosols have the same density: $\rho = 1.5\,\mathrm{kg\,m^{-3}} \times 10^3\,\mathrm{kg\,m^{-3}}$, except the mineral dust with $\rho = 2.65\,\mathrm{kg\,m^{-3}} \times 10^3\,\mathrm{kg\,m^{-3}}$. Δz_k the model layer thickness (for a total of nlevels levels) and $D_{\mathrm{p,min}}$ and $D_{\mathrm{p,max}}$ the minimum and maximum mean mass median diameter of the ith bin. These diameters are converted to radius for the direct comparison with the AERONET data. The naero model species are those presented in the previous sections: SOA, ammonium, nitrate, sulphate, sea salt, PPM, POM, EC and dust.

9.2 Results

Retrieved aerosols size distribution are presented in Fig. 18 for some stations listed in Table 1: Banizoumbou, Cinzana, Capo Verde, Izana and Lampedusa. The aerosols size are expressed in radius, as the original AERONET ASD data. On the Figures, the scale for the volume size distribution changes for each date and site, in order to clearly see the values.

ACPD
15, 3063–3125, 2015

Maximum concentrations are observed and modelled in Banizoumbou and Cinzana, these stations being close to the sources. This also explains that the size distribution is mainly constituted by a mode with $r = 1$ to 2 µm, corresponding to a dominant mode in mineral dust emissions, (Alfaro and Gomes, 2001). For these two sites, a systematic difference is observed between the model and the measurements: the main peak of the modelled coarse mode is for radius of ≈ 1 µm, when the AERONET ASD exhibits a peak for a radius of ≈ 2 µm. This bias will probably induce a longer transport in the model than in reality, since the deposition velocity increases with the aerosols radius for these particles sizes, (Forêt et al., 2006). These results clearly show that improvements have to be done in the size distribution of mineral dust emissions.

After some transport of mineral dust, an important fine mode (with $r \approx 0.03$ µm) is modelled at Capo Verde. This fine fraction is not present in the AERONET size distribution. Far from the mineral dust sources, in Izana and Lampedusa, the comparisons of observed and modelled size distribution are poor. In Izana, the model overestimates the AERONET concentrations for all modes. In Lampedusa, observations clearly show two modes (with radius ≈ 0.1 and 2 µm), when the model reproduces a flat distribution for the 17 June and a coarse mode peak only for the 21 June.

10 Conclusions

This study analyzed the ozone and aerosols tropospheric concentrations and their variability over the Euro-Mediterranean region, from the 1 June to the 15 July 2013. This region and period was the framework of the ADRIMED project, a measurements campaign of the CHARMEX program. This analysis was performed by using measurements from the ADRIMED project (airborne measurements), routine network measurements (AIRBASE, AERONET, E-OBS) and modelling with WRF and CHIMERE. First, the model results were compared to measurements to quantify the ability of the model to restitute the spatio-temporal variability of ozone and aerosols both at the surface and in altitude. Second, the model was used to go further by analyzing the chemical composi-

ACPD
15, 3063–3125, 2015

tion of the aerosols. In addition, the aerosols size distribution variability between Africa and the Mediterranean area was analyzed by comparing AERONET and CHIMERE values.

Meteorological variables such as 2 m temperature and daily precipitation amount were first analyzed using E-OBS data and WRF model results. When measurements are available, it was shown that model and measurements are close in term of daily variability, even if the model has a bias of ≈ -1.5 K over land (where E-OBS data are available). In altitude, and in comparison with aircraft ADRIMED measurements, this variable was found to be correctly modelled. The analysis of the temperature and precipitation showed the summer was with moderate surface temperatures over Europe and two major precipitation events were observed during the period.

The second step was to compare surface ozone and PM_{10} concentrations between model and measurements (from AIRBASE network and ADRIMED specific measurements done at Lampedusa and Cape Corsica). The error statistics showed that the model is able to reproduce surface ozone concentrations, both the average values and the variability, even if we note an overestimation of mean surface ozone concentrations. The comparison between modelled and measured ozone concentrations along the flight trajectories is correct and confirm the high ozone concentration close to the sea surface that are commonly simulated in chemistry transport models. Using the model, it was shown that the ozone plumes were numerous and relatively thin, but not very concentrated, flowing from west to east in Europe. When precipitation events occured, the ozone and PM surface concentations decreased, showing the high impact of photolysis attenuation due to cloudiness for ozone and wet scavenging for aerosols.

It was shown that the period from the 1 June to the 15 July 2013 was not highly polluted. The meteorological conditions were far from drought and precipitation events were non negligible. In addition, this was not a summer under severe vegetation fires events. The most important aerosols events were observed around 16 and 25 June, 4 July 2013. Using the model aerosols speciation, it was shown that the main part of the PM_{10} surface concentration is composed of mineral dust. Another large fraction is

ACPD
15, 3063–3125, 2015

due to sea salt and sulphates concentrations. On the vertical, the mineral dust clearly dominates the total load of aerosols, when sea salt and sulphates are mainly present in the boundary layer. A focus was done on aerosols size distribution by using AERONET products time series over numerous sites, in Africa, close to the sources of mineral dust, and in Europe, where a mix of several sources is present: local erosion, anthropogenic and biogenic emissions, vegetation fires. The ability of the model to reproduce the aerosol size distribution was quantified and it was shown that, close to the source, the coarse mode is understimated when, far from the main desert sources, the fine mode is mainly overestimated by the model.

Acknowledgements. This study was partly funded by the French Ministry in charge of Ecology. We thank the SAFIRE joint laboratory and the CHARMEX program for providing us all campaign measurements used in this study. We thank the EEA for maintaining and providing the AirBase database of pollutants surface concentrations over Europe. We thank the principal investigators and their staff for establishing and maintaining the AERONET sites used in this study: Didier Tanré for Banizoumbou, Capo Verde and Dakar; Bernadette Chatenet and Jean-Louis Rajot for Zinder and Cinzana; Daniela Meloni and Alcide Di Sarra for Lampedusa. We acknowledge the Service d'Observation PHOTONS/AERONET and the AERONET-ACTRIS TNA supporting the AERONET activity in Europe. Analyses and visualizations used in this study for the MODIS satellite AOD maps were produced with the Giovanni online data system, developed and maintained by the NASA GES DISC. We acknowledge the E-OBS dataset from the EU-FP6 project ENSEMBLES (http://ensembles-eu.metoffice.com) and the data providers in the ECAD project (http://www.ecad.eu).

References

Alfaro, S. C. and Gomes, L.: Modeling mineral aerosol production by wind erosion: emission intensities and aerosol size distribution in source areas, J. Geophys. Res., 106, 18075–18084, 2001. 3087, 3088

Barnaba, F. and Gobbi, G. P.: Aerosol seasonal variability over the Mediterranean region and relative impact of maritime, continental and Saharan dust particles over the basin from

ACPD
15, 3063–3125, 2015

MODIS data in the year 2001, Atmos. Chem. Phys., 4, 2367–2391, doi:10.5194/acp-4-2367-2004, 2004. 3066, 3080
Basart, S., Pérez, C., Cuevas, E., Baldasano, J. M., and Gobbi, G. P.: Aerosol characterization in Northern Africa, Northeastern Atlantic, Mediterranean Basin and Middle East from direct-sun AERONET observations, Atmos. Chem. Phys., 9, 8265–8282, doi:10.5194/acp-9-8265-2009, 2009. 3067
Bergamo, A., Tafuro, A. M., Kinne, S., De Tomasi, F., and Perrone, M. R.: Monthly-averaged anthropogenic aerosol direct radiative forcing over the Mediterranean based on AERONET aerosol properties, Atmos. Chem. Phys., 8, 6995–7014, doi:10.5194/acp-8-6995-2008, 2008. 3067
Bessagnet, B., Hodzic, A., Vautard, R., Beekmann, M., Cheinet, S., Honoré, C., Liousse, C., and Rouil, L.: Aerosol modeling with CHIMERE: preliminary evaluation at the continental scale, Atmos. Environ., 38, 2803–2817, 2004. 3072
Bian, H. and Prather, M.: Fast-J2: accurate simulation of stratospheric photolysis in global chemical models, J. Atmos. Chem., 41, 281–296, 2002. 3072
Briant, R., Menut, L., Siour, G., and Prigent, C.: Homogeneized modeling of mineral dust emissions over Europe and Africa using the CHIMERE model, Geosci. Model Dev. Discuss., 7, 3441–3480, doi:10.5194/gmdd-7-3441-2014, 2014. 3073
Chen, F. and Dudhia, J.: Coupling an advanced land surface-hydrology model with the Penn State-NCAR MM5 modeling system. Part I: Model implementation and sensitivity, Mon. Weather Rev., 129, 569–585, 2001. 3071
Colette, A., Ancellet, G., Menut, L., and Arnold, S. R.: A Lagrangian analysis of the impact of transport and transformation on the ozone stratification observed in the free troposphere during the ESCOMPTE campaign, Atmos. Chem. Phys., 6, 3487–3503, doi:10.5194/acp-6-3487-2006, 2006. 3066
Cros, B., Durand, P., Cachier, H., Drobinski, P., Fréjafon, E., Kottmeir, C., Perros, P., Peuch, V.-H., Ponche, J.-L., Robin, D., Said, F., Toupance, G., and Wortham, H.: The ESCOMPTE program: an overview, Atmos. Res., 69, 241–279, 2004. 3066
de la Paz, D., Vedrenne, M., Borge, R., Lumbreras, J., de Andrés, J. M., Pérez, J., Rodriguez, E., Karanasiou, A., Moreno, T., Boldo, E., and Linares, C.: Modelling Saharan dust transport into the Mediterranean basin with CMAQ, Atmos. Environ., 70, 337–350, doi:10.1016/j.atmosenv.2013.01.013, 2013. 3067

ACPD
15, 3063–3125, 2015

di Sarra, A., Pace, G., Meloni, D., De Silvestri, L., Piacentino, S., and Monteleone, F.: Surface shortwave radiative forcing of different aerosol types in the central Mediterranean, Geophys. Res. Lett., 35, doi:10.1029/2007GL032395, 2008. 3067

Dubovik, O. and King, M. D.: A flexible inversion algorithm for retrieval of aerosol optical properties from Sun and sky radiance measurements, J. Geophys. Res.-Atmos., 105, 20673–20696, doi:10.1029/2000JD900282, 2000. 3070, 3086

Dulac, F. and Chazette, P.: Airborne study of a multi-layer aerosol structure in the eastern Mediterranean observed with the airborne polarized lidar ALEX during a STAAARTE campaign (7 June 1997), Atmos. Chem. Phys., 3, 1817–1831, doi:10.5194/acp-3-1817-2003, 2003. 3066

Dulac, F., Arboledas, L. A., Alastuey, A., Ancellet, G., Arndt, J., Attié, J.-L., Augustin, P., Becagli, S., Bergametti, G., Bocquet, M., Bordier, F., Bourdon, A., Bourrianne, T., Bravo-Aranda, J., Carrer, D., Ceamanos, X., Chazette, P., Chiapello, I., Comeron, A., D'Amico, G., D'Anna, B., Delbarre, H., Denjean, C., Desboeufs, K., Descloitres, J., Diouri, M., Biagio, C. D., Iorio, T. D., Sarra, G. D., Doppler, L., Durand, P., Amraoui, L. E., Ellul, R., Ferré, H., Fleury, L., Formenti, P., Freney, E., Gaimoz, C., Gerasopoulos, E., Goloub, P., Gomez-Amo, J., Granados-Munoz, M., Grand, N., Grobner, J., Rascado, J.-L. G., Guieu, C., Hadjimitsis, D., Hamonou, E., Hansson, H., Iarlori, M., Ioannou, S., Jambert, C., Jaumouillé, E., Jeannot, M., Junkermann, W., Keleshis, C., Kokkalis, P., Lambert, D., Laurent, B., Léon, J.-F., Liousse, C., Bartolome, M. L., Losno, R., Mallet, M., Mamouri, R.-E., Meloni, D., Menut, L., Montoux, N., Baquero, R. M., Nabat, P., Navas-Guzman, F., Nicolae, D., Nicolas, J., Notton, G., Ohayon, W., Paoli, C., Papayannis, A., Pelon, J., Pey, J., Pont, V., Pujadas, M., Querol, X., Ravetta, F., Renard, J.-B., Rizi, V., Roberts, G., Roujean, J.-L., Sartelet, K., Savelli, J.-L., Sciare, J., Sellegri, K., Sferlazzo, D., Sicard, M., Smyth, A., Solmon, F., Tanré, D., Torres, B., Totems, J., Sanchez, A. T., Verdier, N., Vignelles, D., Vincent, J., Wagner, F., Wang, Y., Wenger, J., and Yassaa, N.: Overview of the Project ChArMEx activities on Saharan Dust in the Mediterranean region, in: 7th Int. Workshop on Sand/Duststorms and Associated Dustfall, 2–4 Dec. 2013, Frascati, Italy, 2013. 3066

Forêt, G., Bergametti, G., Dulac, F., and Menut, L.: An optimized particle size bin scheme for modeling mineral dust aerosol, J. Geophys. Res., 111, D17310, doi:10.1029/2005JD006797, 2006. 3088

ACPD
15, 3063–3125, 2015

Gerasopoulos, E., Kouvarakis, G., Vrekoussis, M., Kanakidou, M., and Mihalopoulos, N.: Ozone variability in the marine boundary layer of the eastern Mediterranean based on 7-year observations, J. Geophys. Res., 110, D15309, 2005. 3066

Ginoux, P., Chin, M., Tegen, I., Prospero, J. M., Holben, B., Dubovik, O., and Lin, S. J.: Sources and distributions of dust aerosols simulated with the GOCART model, J. Geophys. Res., 106, 20255–20273, 2001. 3072

Grell, G. A. and Devenyi, D.: A generalized approach to parameterizing convection combining ensemble and data assimilation techniques, Geophys. Res. Lett., 29, 1693, doi:10.1029/2002GL015311, 2002. 3071

Guenther, A., Karl, T., Harley, P., Wiedinmyer, C., Palmer, P. I., and Geron, C.: Estimates of global terrestrial isoprene emissions using MEGAN (Model of Emissions of Gases and Aerosols from Nature), Atmos. Chem. Phys., 6, 3181–3210, doi:10.5194/acp-6-3181-2006, 2006. 3073

Guerreiro, C., de Leuw, F., and Foltescu, V.: Air quality in Europe, European Environment Agency, report, 9, 112, 2013. 3069

Haylock, M. R., Hofstra, N., Tank, A. M. G. K., Klok, E. J., Jones, P. D., and New, M.: A European daily high-resolution gridded data set of surface temperature and precipitation for 1950–2006, J. Geophys. Res.-Atmos., 113, doi:10.1029/2008JD010201, 2008. 3069

Holben, B., Tanre, D., Smirnov, A., Eck, T. F., Slutsker, I., Abuhassan, N., Newcomb, W. W., Schafer, J., Chatenet, B., Lavenu, F., Kaufman, Y. J., Vande Castle, J., Setzer, A., Markham, B., Clark, D., Frouin, R., Halthore, R., Karnieli, A., O'Neill, N. T., Pietras, C., Pinker, R. T., Voss, K., and Zibordi, G.: An emerging ground-based aerosol climatology: aerosol optical depth from AERONET, J. Geophys. Res., 106, 12067–12097, 2001. 3070, 3081

Hong, S. Y., Dudhia, J., and Chen, S.: A revised approach to ice microphysical processes for the bulk parameterization of clouds and precipitation, Mon. Weather Rev., 132, 103–120, 2004. 3071

Hong, S. Y., Noh, Y., and Dudhia, J.: A new vertical diffusion package with an explicit treatment of entrainment processes, Mon. Weather Rev., 134, 2318–2341, doi:10.1175/MWR3199.1, 2006. 3071

Israelevich, P., Ganor, E., Alpert, P., Kishcha, P., and Stupp, A.: Predominant transport paths of Saharan dust over the Mediterranean Sea to Europe, J. Geophys. Res., 117, D02205, 2012. 3065

ACPD
15, 3063–3125, 2015

Jiménez-Guerrero, P., Jorba, O., Pay, M. T., Montávez, J. P., Jerez, S., Gómez-Navarro, J. J., and Baldasano, J. M.: Comparison of two different sea-salt aerosol schemes as implemented in air quality models applied to the Mediterranean Basin, Atmos. Chem. Phys., 11, 4833–4850, doi:10.5194/acp-11-4833-2011, 2011. 3067

Kalabokas, P., Mihalopoulos, N., Ellul, R., Kleanthous, S., and Repapis, C.: An investigation of the meteorological and photochemical factors influencing the background rural and marine surface ozone levels in the Central and Eastern Mediterranean, Atmos. Environ., 42, 7894–7906, doi:10.1016/j.atmosenv.2008.07.009, 2008. 3066

Kubilay, N., Cokacar, T., and Oguz, T.: Optical properties of mineral dust outbreaks over the northeastern Mediterranean, J. Geophys. Res., 108, 4666, 2003. 3065, 3066

Kulmala, M., Asmi, A., Lappalainen, H. K., Baltensperger, U., Brenguier, J.-L., Facchini, M. C., Hansson, H.-C., Hov, Ø., O'Dowd, C. D., Pöschl, U., Wiedensohler, A., Boers, R., Boucher, O., de Leeuw, G., Denier van der Gon, H. A. C., Feichter, J., Krejci, R., Laj, P., Lihavainen, H., Lohmann, U., McFiggans, G., Mentel, T., Pilinis, C., Riipinen, I., Schulz, M., Stohl, A., Swietlicki, E., Vignati, E., Alves, C., Amann, M., Ammann, M., Arabas, S., Artaxo, P., Baars, H., Beddows, D. C. S., Bergström, R., Beukes, J. P., Bilde, M., Burkhart, J. F., Canonaco, F., Clegg, S. L., Coe, H., Crumeyrolle, S., D'Anna, B., Decesari, S., Gilardoni, S., Fischer, M., Fjaeraa, A. M., Fountoukis, C., George, C., Gomes, L., Halloran, P., Hamburger, T., Harrison, R. M., Herrmann, H., Hoffmann, T., Hoose, C., Hu, M., Hyvärinen, A., Hõrrak, U., Iinuma, Y., Iversen, T., Josipovic, M., Kanakidou, M., Kiendler-Scharr, A., Kirkevåg, A., Kiss, G., Klimont, Z., Kolmonen, P., Komppula, M., Kristjánsson, J.-E., Laakso, L., Laaksonen, A., Labonnote, L., Lanz, V. A., Lehtinen, K. E. J., Rizzo, L. V., Makkonen, R., Manninen, H. E., McMeeking, G., Merikanto, J., Minikin, A., Mirme, S., Morgan, W. T., Nemitz, E., O'Donnell, D., Panwar, T. S., Pawlowska, H., Petzold, A., Pienaar, J. J., Pio, C., Plass-Duelmer, C., Prévôt, A. S. H., Pryor, S., Reddington, C. L., Roberts, G., Rosenfeld, D., Schwarz, J., Seland, Ø., Sellegri, K., Shen, X. J., Shiraiwa, M., Siebert, H., Sierau, B., Simpson, D., Sun, J. Y., Topping, D., Tunved, P., Vaattovaara, P., Vakkari, V., Veefkind, J. P., Visschedijk, A., Vuollekoski, H., Vuolo, R., Wehner, B., Wildt, J., Woodward, S., Worsnop, D. R., van Zadelhoff, G.-J., Zardini, A. A., Zhang, K., van Zyl, P. G., Kerminen, V.-M., S Carslaw, K., and Pandis, S. N.: General overview: European Integrated project on Aerosol Cloud Climate and Air Quality interactions (EUCAARI) – integrating aerosol research from nano to global scales, Atmos. Chem. Phys., 11, 13061–13143, doi:10.5194/acp-11-13061-2011, 2011. 3067

ACPD
15, 3063–3125, 2015

Lelieveld, J., Berresheim, H., Borrmann, S., Crutzen, P. J., Dentener, F. J., Fischer, H., Feichter, J., Flatau, P. J., Heland, J., Holzinger, R., Korrmann, R., Lawrence, M. G., Levin, Z., Markowicz, K. M., Mihalopoulos, N., Minikin, A., Ramanathan, V., Reus, M. d., Roelofs, G. J., Scheeren, H. A., Sciare, J., Schlager, H., Schultz, M., Siegmund, P., Steil, B., Stephanou, E. G., Stier, P., Traub, M., Warneke, C., Williams, J., and Ziereis, H.: Global air pollution crossroads over the Mediterranean, Science, 298, 794–799, 2002. 3066

Levy, R. C., Remer, L. A., Kleidman, R. G., Mattoo, S., Ichoku, C., Kahn, R., and Eck, T. F.: Global evaluation of the Collection 5 MODIS dark-target aerosol products over land, Atmos. Chem. Phys., 10, 10399–10420, doi:10.5194/acp-10-10399-2010, 2010. 3080

Mailler, S.: On the radiative impact of aerosols on photolysis rates: comparison of simulations and observations in the Lampedusa island during the CharMEx/ADRIMED campaign, Atmos. Chem. Phys. Discuss., in review, 2015. 3072

Mailler, S., Khvorostyanov, D., and Menut, L.: Impact of the vertical emission profiles on background gas-phase pollution simulated from the EMEP emissions over Europe, Atmos. Chem. Phys., 13, 5987–5998, doi:10.5194/acp-13-5987-2013, 2013. 3073

Mallet M. et al, The Aerosol Direct Radiative Impact in the MEDiterranean (ADRIMED) project, Atelier de Modelisation de l'Atmosphere, 21 January 2014, Toulouse, France, http://www.meteo.fr/cic/meetings/2014/AMA/programme.pdf, 2014. Please confirm correction and add all authors. 3066, 3070

Mallet, M., Dubovik, O., Nabat, P., Dulac, F., Kahn, R., Sciare, J., Paronis, D., and Léon, J. F.: Absorption properties of Mediterranean aerosols obtained from multi-year ground-based remote sensing observations, Atmos. Chem. Phys., 13, 9195–9210, doi:10.5194/acp-13-9195-2013, 2013. 3067

Menut, L., Coll, I., and Cautenet, S.: Impact of meteorological data resolution on the forecasted ozone concentrations during the ESCOMPTE IOP 2a and 2b, Atmos. Res., 74, 139–159, 2005. 3067

Menut, L., Goussebaile, A., Bessagnet, B., Khvorostiyanov, D., and Ung, A.: Impact of realistic hourly emissions profiles on modelled air pollutants concentrations, Atmos. Environ., 233–244, 2012. 3072

Menut, L., Bessagnet, B., Khvorostyanov, D., Beekmann, M., Blond, N., Colette, A., Coll, I., Curci, G., Foret, G., Hodzic, A., Mailler, S., Meleux, F., Monge, J.-L., Pison, I., Siour, G., Turquety, S., Valari, M., Vautard, R., and Vivanco, M. G.: CHIMERE 2013: a model for regional

ACPD
15, 3063–3125, 2015

atmospheric composition modelling, Geosci. Model Dev., 6, 981–1028, doi:10.5194/gmd-6-981-2013, 2013a. 3072, 3084, 3087
Menut, L., Perez Garcia-Pando, C., Haustein, K., Bessagnet, B., Prigent, C., and Alfaro, S.: Relative impact of roughness and soil texture on mineral dust emission fluxes modeling, J. Geophys. Res., 118, 6505–6520, doi:10.1002/jgrd.50313, 2013b. 3067, 3073
Menut, L., Tripathi, O., Colette, A., Vautard, R., Flaounas, E., and Bessagnet, B.: Evaluation of regional climate simulations for air quality modelling purposes, Clim. Dynam., 40, 2515–2533, doi:10.1007/s00382-012-1345-9, 2013c. 3073
Middleton, N. J. and Goudie, A. S.: Saharan dust: sources and trajectories, T. I. Brit. Geogr., 26, 165–181, doi:10.1111/1475-5661.00013, 2001. 3065
Millan, M., Estrela, M. J., Sanz, M. J., Mantilla, E., Martan, M., Pastor, F., Salvador, R., Vallejo, R., Alonso, L., Gangoiti, G., Ilardia, J., Navazo, M., Albizuri, A., Artano, B., Ciccioli, P., Kallos, G., Carvalho, R. A., Andreas, D., Hoff, A., Werhahn, J., and Seufert, G., and Versino, B.: Climatic feedbacks and desertification: the Mediterranean Model, J. Climate, 18, 684–701, 2005. 3066
Mlawer, E., Taubman, S., Brown, P., Iacono, M., and Clough, S.: Radiative transfer for inhomogeneous atmospheres: RRTM a validated correlated-k model for the longwave, J. Geophys. Res., 102, 16663–16682, 1997. 3071
Monks, P., Granier, C., Fuzzi, S., Stohl, A., Williams, M., Akimoto, H., Amann, M., Baklanov, A., Baltensperger, U., Bey, I., Blake, N., Blake, R., Carslaw, K., Cooper, O., Dentener, F., Fowler, D., Fragkou, E., Frost, G., Generoso, S., Ginoux, P., Grewe, V., Guenther, A., Hansson, H., Henne, S., Hjorth, J., Hofzumahaus, A., Huntrieser, H., Isaksen, I., Jenkin, M., Kaiser, J., Kanakidou, M., Klimont, Z., Kulmala, M., Laj, P., Lawrence, M., Lee, J., Liousse, C., Maione, M., McFiggans, G., Metzger, A., Mieville, A., Moussiopoulos, N., Orlando, J., O'Dowd, C., Palmer, P., Parrish, D., Petzold, A., Platt, U., Pöschl, U., Prévt, A., Reeves, C., Reimann, S., Rudich, Y., Sellegri, K., Steinbrecher, R., Simpson, D., ten Brink, H., Theloke, J., van der Werf, G., Vautard, R., Vestreng, V., Vlachokostas, C., and von Glasow, R.: Atmospheric composition change – global and regional air quality, Atmos. Environ., 43, 5268–5350, doi:10.1016/j.atmosenv.2009.08.021, 2009. 3066
Moulin, C., Lambert, C. E., Dayan, U., Masson, V., Ramonet, M., Bousquet, P., Legrand, M., Balkanski, Y. J., Guelle, W., Marticorena, B., Bergametti, G., and Dulac, F.: Satellite climatology of African dust transport in the Mediterranean atmosphere, J. Geophys. Res.-Atmos., 103, 13137–13144, doi:10.1029/98JD00171, 1998. 3065

ACPD
15, 3063–3125, 2015

Nabat, P., Solmon, F., Mallet, M., Kok, J. F., and Somot, S.: Dust emission size distribution impact on aerosol budget and radiative forcing over the Mediterranean region: a regional climate model approach, Atmos. Chem. Phys., 12, 10545–10567, doi:10.5194/acp-12-10545-2012, 2012. 3067

Nabat, P., Somot, S., Mallet, M., Sevault, F., Chiacchio, M., and Wild, M.: Direct and semi-direct aerosol radiative effect on the Mediterranean climate variability using a coupled regional climate system model, Clim. Dynam., 1–29, doi:10.1007/s00382-014-2205-6, 2014. 3067

Papayannis, A., Amiridis, V., Mona, L., Tsaknakis, G., Balis, D., Bösenberg, J., Chaikovski, A., De Tomasi, F., Grigorov, I., Mattis, I., Mitev, V., Müller, D., Nickovic, S., Pérez, C., Pietruczuk, A., Pisani, G., Ravetta, F., Rizi, V., Sicard, M., Trickl, T., Wiegner, M., Gerding, M., Mamouri, R. E., D'Amico, G., and Pappalardo, G.: Systematic lidar observations of Saharan dust over Europe in the frame of EARLINET (2000–2002), J. Geophys. Res.-Atmos., 113, 2156–2202, doi:10.1029/2007JD009028, 2008. 3066

Pappalardo, G., Amodeo, A., Apituley, A., Comeron, A., Freudenthaler, V., Linné, H., Ansmann, A., Bösenberg, J., D'Amico, G., Mattis, I., Mona, L., Wandinger, U., Amiridis, V., Alados-Arboledas, L., Nicolae, D., and Wiegner, M.: EARLINET: towards an advanced sustainable European aerosol lidar network, Atmos. Meas. Tech., 7, 2389–2409, doi:10.5194/amt-7-2389-2014, 2014. 3066

Péré, J., Mallet, M., Pont, V., and Bessagnet, B.: Evaluation of an aerosol optical scheme in the chemistry-transport model CHIMERE, Atmos. Environ., 44, 3688–3699, 2010. 3087

Pérez, C., Haustein, K., Janjic, Z., Jorba, O., Huneeus, N., Baldasano, J. M., Black, T., Basart, S., Nickovic, S., Miller, R. L., Perlwitz, J. P., Schulz, M., and Thomson, M.: Atmospheric dust modeling from meso to global scales with the online NMMB/BSC-Dust model – Part 1: Model description, annual simulations and evaluation, Atmos. Chem. Phys., 11, 13001–13027, doi:10.5194/acp-11-13001-2011, 2011. 3067

Querol, X., Pey, J., Pandolfi, M., Alastuey, A., Cusack, M., Pereza, N., Moreno, T., Viana, M., Mihalopoulos, N., Kallo, G., and Kleanthous, S.: African dust contributions to mean ambient PM10 mass-levels across the Mediterranean Basin, Atmos. Environ., 43, 4266–4277, 2009. 3066

Richards, N. A. D., Arnold, S. R., Chipperfield, M. P., Miles, G., Rap, A., Siddans, R., Monks, S. A., and Hollaway, M. J.: The Mediterranean summertime ozone maximum: global emission sensitivities and radiative impacts, Atmos. Chem. Phys., 13, 2331–2345, doi:10.5194/acp-13-2331-2013, 2013. 3067

ACPD
15, 3063–3125, 2015

Roelofs, G. J., Scheeren, H. A., Heland, J., Ziereis, H., and Lelieveld, J.: A model study of ozone in the eastern Mediterranean free troposphere during MINOS (August 2001), Atmos. Chem. Phys., 3, 1199–1210, doi:10.5194/acp-3-1199-2003, 2003. 3066

Santese, M., Perrone, M. R., Zakey, A. S., De Tomasi, F., and Giorgi, F.: Modeling of Saharan dust outbreaks over the Mediterranean by RegCM3: case studies, Atmos. Chem. Phys., 10, 133–156, doi:10.5194/acp-10-133-2010, 2010. 3067

Skamarock, W., Klemp, J., Dudhia, J., Gill, D., Barker, D., Wang, W., and Powers, J.: A Description of the Advanced Research WRF Version 2, NCAR Technical Note, Boulder, Colorado, USA, pp. NCAR/TN–468+STR, 2007. 3071

Spyrou, C., Kallos, G., Mitsakou, C., Athanasiadis, P., Kalogeri, C., and Iacono, M. J.: Modeling the radiative effects of desert dust on weather and regional climate, Atmos. Chem. Phys., 13, 5489–5504, doi:10.5194/acp-13-5489-2013, 2013. 3067

Szopa, S., Foret, G., Menut, L., and Cozic, A.: Impact of large scale circulation on European summer surface ozone: consequences for modeling, Atmos. Environ., 43, 1189–1195, doi:10.1016/j.atmosenv.2008.10.039, 2009. 3072

Turquety, S., Menut, L., Bessagnet, B., Anav, A., Viovy, N., Maignan, F., and Wooster, M.: APIFLAME v1.0: high-resolution fire emission model and application to the Euro-Mediterranean region, Geosci. Model Dev., 7, 587–612, doi:10.5194/gmd-7-587-2014, 2014. 3067, 3073

Vogel, B., Vogel, H., Bäumer, D., Bangert, M., Lundgren, K., Rinke, R., and Stanelle, T.: The comprehensive model system COSMO-ART – Radiative impact of aerosol on the state of the atmosphere on the regional scale, Atmos. Chem. Phys., 9, 8661–8680, doi:10.5194/acp-9-8661-2009, 2009. 3067

Von Storch, H., Langenberg, H., and Feser, F.: A spectral nudging technique for dynamical downscaling purposes, Mon. Weather Rev., 128, 3664–3673, 2000. 3071

Vuolo, M., Chepfer, H., Menut, L., and Cezana, G.: Comparison of mineral dust layers vertical structures modelled with CHIMERE-DUST and observed with the CALIOP lidar, J. Geophys. Res., 114, D09214, doi:10.1029/2008JD011219, 2009. 3083

Wild, O., Zhu, X., and Prather, M. J.: Fast-J: accurate simulation of in- and below-cloud photolysis in tropospheric chemical models, J. Atmos. Chem., 37, 245–282, 2000. 3072

ACPD
15, 3063–3125, 2015

Table 1. Characteristics of the AirBase and AERONET stations used in this study. Note that the AirBase Italian stations of Chitignano, Baceno, Schivenoglia and Vercelli provide daily averaged values, when all other stations provide hourly (but not regular) measurements. The altitude is in meters and above sea level (a.s.l.).

Site	Country	Longitude (°)	Latitude (°)	Altitude (m a.s.l.)
ADRIMED measurements sites				
Lampedusa	Italy	12.63	35.51	45.
Cape Corsica	France	9.41	42.83	533.
AirBase coastal "background" stations				
Zorita	Spain	−0.16	40.73	619.
Cartagena	Spain	−0.97	37.60	10.
Malaga	Spain	−4.46	36.72	36.
Ajaccio	France	8.73	41.92	28.
Bastia	France	9.44	42.69	57.
Hyeres	France	6.13	43.11	33.
Taranto	Italy	17.28	40.41	10.
Chitignano	Italy	11.90	43.66	650.
AirBase continental "background" stations				
Aranjuez	Spain	−3.59	40.04	501.
Logrono	Spain	−2.42	42.46	386.
Cordoba	Spain	−4.77	37.90	119.
Agen	France	0.62	44.19	50.
Champforgeuil	France	4.83	46.82	46.
Gap	France	6.07	44.55	741.
Baceno	Italy	8.25	46.31	1637.
Schivenoglia	Italy	11.07	44.99	16.
Vercelli	Italy	8.40	45.31	131.
AERONET stations				
Banizoumbou	Nigeria	2.66	13.54	250.
Capo Verde	Capo Verde	−22.93	16.73	60.
Dakar	Senegal	−16.95	14.39	0.
Cinzana	Mali	−5.93	13.28	285.
Ilorin	Nigeria	4.340	8.32	350.
Izana	Spain	−16.49	28.31	2391.
Forth Crete	Greece	25.27	35.31	20.
Saada	Morocco	−8.15	31.61	420.
Zinder Airport	Nigeria	8.98	13.75	456.

ACPD
15, 3063–3125, 2015

Table 2. List of ATR flights for the tropospheric measurements of meteorological variables and ozone concentrations. N_{data} corresponds to the number of data after averaging the high temporal frequency of aircraft measurements to a constant 5 mn time step.

Flight n°	Date	J_{day}	Decimal hour	N_{data}
28	20130614	165	9.05	46
29	20130616	167	7.55	36
30	20130616	167	11.49	40
31	20130617	168	6.76	39
32	20130617	168	11.18	32
33	20130619	170	11.04	49
34	20130620	171	9.83	54
35	20130622	173	7.57	47
36	20130622	173	12.75	40

ACPD
15, 3063–3125, 2015

Table 3. Correlations (R), Root Mean Squared Error (RMSE) and bias of measured and modelled daily mean averaged values of 2 m temperature (K). The bias expressed the (model) minus (observations) values.

Site	$T_{2\,m}$ daily mean (K)		R	RMSE	bias
	Obs	Mod			
Cape Corsica	293.18	292.26	0.89	1.54	−0.92
Zorita	293.22	291.41	0.87	2.54	−1.81
Bastia	291.55	292.42	0.90	1.46	0.87
Chitignano	293.61	291.63	0.94	2.19	−1.98
Aranjuez	297.33	295.63	0.99	1.83	−1.70
Logrono	290.00	287.88	0.96	2.42	−2.11
Cordoba	298.15	296.20	0.98	2.06	−1.96
Agen	293.11	291.90	0.95	1.64	−1.20
Champforgeuil	292.64	289.25	0.96	3.50	−3.39
Gap	289.61	287.59	0.96	2.21	−2.02
Baceno	287.89	283.80	0.95	4.21	−4.10
Schivenoglia	296.28	294.17	0.96	2.26	−2.12
Vercelli	295.51	292.46	0.95	3.17	−3.05

ACPD
15, 3063–3125, 2015

Table 4. Hit rate (HR) and bias of measured and modelled daily mean averaged values of precipitation amount (mm day^{-1}). The bias expressed the (model) minus (observations) values.

Site	Nobs	Pr (mm day^{-1})		HR	bias
		Obs	Mod		
Cape Corsica	3	2.10	0.97	0.67	−1.13
Zorita	4	9.68	6.38	1.00	−3.29
Bastia	3	4.73	5.18	0.67	0.45
Chitignano	6	4.12	3.79	0.83	−0.33
Aranjuez	1	1.20	0.93	1.00	−0.27
Logrono	11	6.73	5.73	1.00	−1.00
Cordoba	1	1.40	0.11	1.00	−1.29
Agen	14	7.16	2.91	0.64	−4.25
Champforgeuil	13	7.12	4.11	0.92	−3.01
Gap	8	6.53	9.41	0.75	2.89
Baceno	19	4.73	11.95	1.00	7.22
Schivenoglia	6	6.87	2.44	0.83	−4.42
Vercelli	9	5.59	3.30	0.67	−2.29

ACPD
15, 3063–3125, 2015

Table 5. Correlations (R), Root Mean Squared Error (RMSE) and bias of measured and modelled daily maximum value of surface O_3 concentrations ($\mu g\,m^{-3}$), for representative AirBase stations.

Site	N_{obs}	O_3 daily max		R	RMSE	bias
		Obs	Mod			
AirBase coastal "background" stations						
Zorita	37	110.6	105.0	0.66	14.8	−5.6
Cartagena	41	102.4	113.1	0.47	16.2	10.7
Malaga	40	113.6	101.0	0.15	24.2	−12.6
Ajaccio	38	107.2	100.9	0.39	18.0	−6.3
Bastia	41	114.8	97.3	0.21	25.0	−17.5
Hyeres	41	118.6	95.7	0.55	29.3	−22.9
Taranto	41	116.8	123.3	0.70	12.8	6.5
Chitignano	40	99.4	110.2	0.56	20.5	10.8
AirBase continental "background" stations						
Aranjuez	38	113.3	112.2	0.38	22.0	−1.0
Lograno	41	102.3	97.5	0.55	21.6	−4.9
Cordoba	41	127.3	113.1	0.60	21.0	−14.2
Agen	41	95.3	95.8	0.71	19.3	0.5
Champforgeuil	38	99.3	99.5	0.54	21.3	0.3
Gap	39	98.4	103.9	0.32	16.8	5.6
Baceno	39	117.0	104.6	0.29	21.5	−12.4
Vercelli	39	124.4	129.2	0.61	26.0	4.8

ACPD
15, 3063–3125, 2015

Table 6. Correlations (R), Root Mean Squared Error (RMSE) and bias of measured and modelled of hourly surface O_3 concentrations ($\mu g\,m^{-3}$), for representative AirBase stations.

Site	N_{obs}	O_3 hourly		R	RMSE	bias
		Obs	Mod			
AirBase coastal "background" stations						
Zorita	815	74.0	84.7	0.71	28.2	10.7
Cartagena	956	73.4	93.9	0.59	29.7	20.5
Malaga	907	87.2	87.4	0.40	23.5	0.2
Ajaccio	892	73.0	79.8	0.40	26.1	6.8
Bastia	978	90.8	76.4	0.29	27.8	−14.4
Hyeres	983	86.5	68.2	0.64	29.1	−18.3
Taranto	575	90.1	98.5	0.74	19.0	8.4
Chitignano	892	72.4	89.4	0.55	27.6	17.0
AirBase continental "background" stations						
Aranjuez	841	79.7	82.9	0.67	21.3	3.2
Lograno	978	72.3	79.1	0.66	22.9	6.8
Cordoba	945	91.0	89.4	0.81	17.2	−1.6
Agen	977	64.6	74.9	0.73	23.0	10.3
Champforgeuil	836	61.9	76.2	0.67	31.1	14.3
Gap	917	66.1	91.4	0.36	35.5	25.3
Baceno	913	86.3	91.3	0.62	19.6	5.1
Vercelli	898	85.1	93.1	0.68	26.8	8.0

ACPD
15, 3063–3125, 2015

Table 7. Correlations (R), Root Mean Squared Error (RMSE) and bias of measured and modelled hourly Aerosol Optical Depth, for the AERONET stations.

Site	N_{obs}	$\overline{\text{AOD}}$ hourly		R	RMSE	bias
		Obs	Mod			
Banizoumbou	357	0.59	0.46	0.27	0.49	−0.12
Capo Verde	166	0.49	0.46	0.50	0.16	−0.03
Dakar	248	0.53	0.65	0.55	0.23	0.13
Cinzana	338	0.58	0.45	0.58	0.34	−0.13
Ilorin	104	0.38	0.42	0.20	0.35	0.04
Izana	516	0.05	0.15	0.77	0.15	0.10
Lampedusa	238	0.16	0.22	0.79	0.09	0.06
Saada	410	0.24	0.24	0.65	0.15	0.00
Zinder Airport	345	0.56	0.69	0.41	0.43	0.13
Forth Crete	108	0.11	0.17	0.49	0.08	0.06

ACPD
15, 3063–3125, 2015

Table 8. Correlation (R), bias and RMSE for the daily mean averaged PM_{10} ($\mu g\,m^{-3}$) surface concentrations (except for the Lampedusa measurements corresponding to Total Suspended Particles).

Site	N_{obs}	PM_{10} daily mean		R	RMSE	bias
		Obs	Mod			
AirBase coastal "background" stations						
Zorita	37	16.1	15.5	0.59	8.9	−0.5
Cartagena	41	21.6	23.1	−0.02	12.7	1.5
Malaga	40	32.5	30.1	−0.09	20.0	−2.4
Ajaccio	33	21.0	27.6	0.15	11.2	6.6
Bastia	40	21.1	25.0	0.09	9.5	3.9
Hyeres	41	29.2	25.9	0.68	6.3	−3.3
Taranto	39	19.8	21.4	0.48	7.0	1.6
Chitignano	40	10.4	20.3	0.66	10.8	10.0
AirBase continental "background" stations						
Aranjuez	38	23.1	14.3	0.41	12.8	−8.8
Logrono	41	23.2	14.7	0.46	10.1	−8.5
Cordoba	41	21.2	23.4	0.23	18.1	2.2
Agen	41	14.5	16.6	−0.04	9.7	2.1
Champforgeuil	41	15.8	17.5	0.17	9.7	1.6
Gap	35	13.0	13.5	0.56	4.9	0.5
Baceno	33	7.9	12.6	0.38	8.7	4.8
Schivenoglia	39	27.5	20.6	0.32	12.1	−6.8
Vercelli	36	16.3	19.2	0.68	7.2	2.9

ACPD
15, 3063–3125, 2015

Table 9. Relative percentages of the chemical composition of the modelled surface PM_{10} for each site. Values are calculated using the hourly values for the period from the 1 June to the 15 July 2013. For each site, the largest value is bolded.

Site	SOA	Ammonium	Nitrate	Sulphate	Sea salt	PPM	POM	EC	Dust
AirBase coastal "background" stations									
Lampedusa	6.17	6.60	0.70	20.20	23.71	2.95	2.86	1.06	**35.75**
Cape Corsica	12.26	10.51	2.57	**28.39**	10.77	5.18	6.95	2.70	20.66
Zorita	5.12	7.20	0.79	19.43	5.95	2.70	2.16	0.74	**55.90**
Cartagena	3.76	6.92	0.71	19.16	19.28	2.74	3.27	1.25	**42.92**
Malaga	3.20	6.12	2.74	14.97	19.35	3.62	4.17	1.64	**44.20**
Ajaccio	13.91	9.40	5.92	**22.79**	11.94	5.96	12.36	4.85	12.88
Bastia	14.36	10.74	2.64	**28.05**	7.84	5.48	7.71	2.99	20.20
Hyeres	7.05	6.69	2.65	18.54	12.56	10.56	**23.79**	9.57	8.59
Taranto	9.25	9.21	0.45	25.75	14.21	7.38	4.27	1.69	**27.79**
Chitignano	15.87	10.54	3.67	**26.16**	4.78	7.51	6.50	2.59	22.39
AirBase continental "background" stations									
Aranjuez	3.80	6.69	0.83	17.52	5.50	4.07	3.43	0.93	**57.23**
Logrono	10.03	10.82	4.22	28.25	6.76	3.19	2.34	0.80	**33.60**
Cordoba	2.73	5.39	0.40	14.34	7.29	2.50	2.18	0.68	**64.48**
Agen	9.36	9.67	3.47	24.56	12.76	5.06	3.39	1.35	**30.39**
Champforgeuil	11.46	11.13	8.17	24.93	7.25	6.58	3.79	1.69	**25.01**
Gap	12.68	10.27	4.17	25.63	3.85	6.35	4.07	1.75	**31.24**
Baceno	12.82	10.81	9.39	23.35	2.00	4.89	3.51	1.43	**31.81**
Schivenoglia	14.03	11.04	7.89	**24.73**	3.77	7.93	6.32	2.66	21.63
Vercelli	13.58	9.64	3.17	24.40	2.68	9.08	6.85	2.93	**27.65**

ACPD
15, 3063–3125, 2015

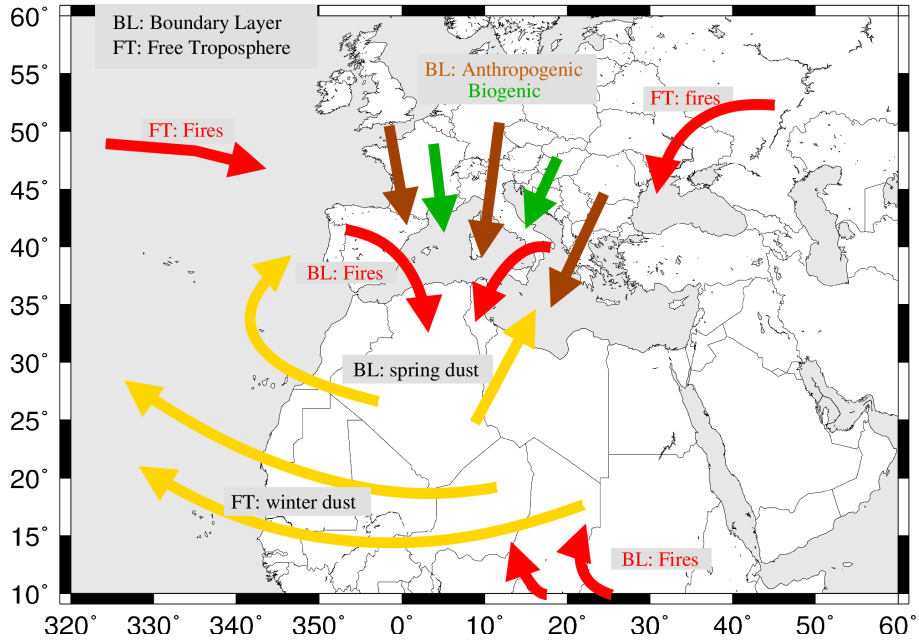

Figure 1. Synthesis of all aerosols types and transport pathways in the Mediterranean area. BL and FT stand for "boundary layer" and "free troposphere", respectively.

ACPD
15, 3063–3125, 2015

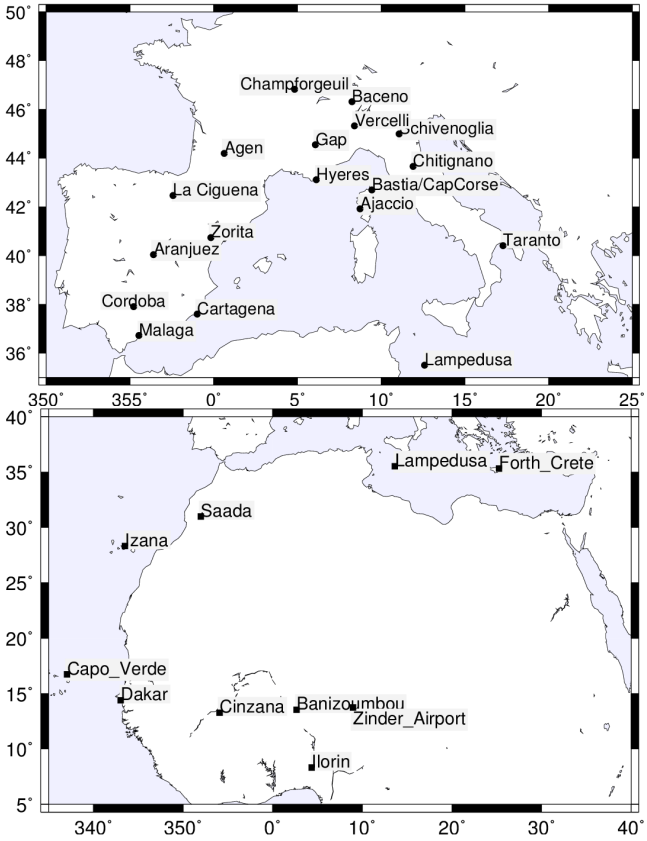

Figure 2. Locations of the AirBase (top) and AERONET (bottom) stations providing the O_3, PM_{10}, aerosols optical depth (AOD) and aerosols size distributions (ASD) measurements used in this study.

ACPD
15, 3063–3125, 2015

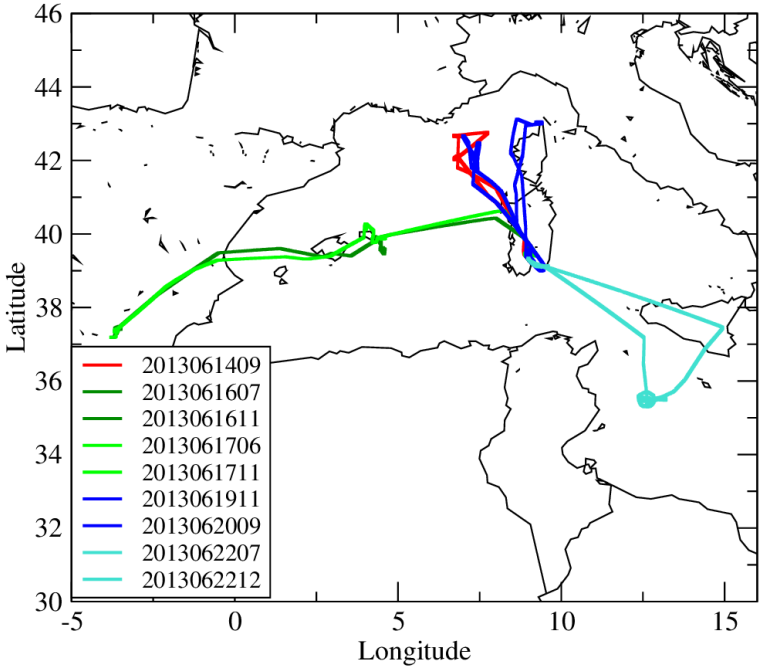

Figure 3. ATR-42 horizontal trajectories for the flight of the 14 June (red), 16 and 17 June (blue), 19 and 20 June (green) and 22 June (green-blue).

ACPD
15, 3063–3125, 2015

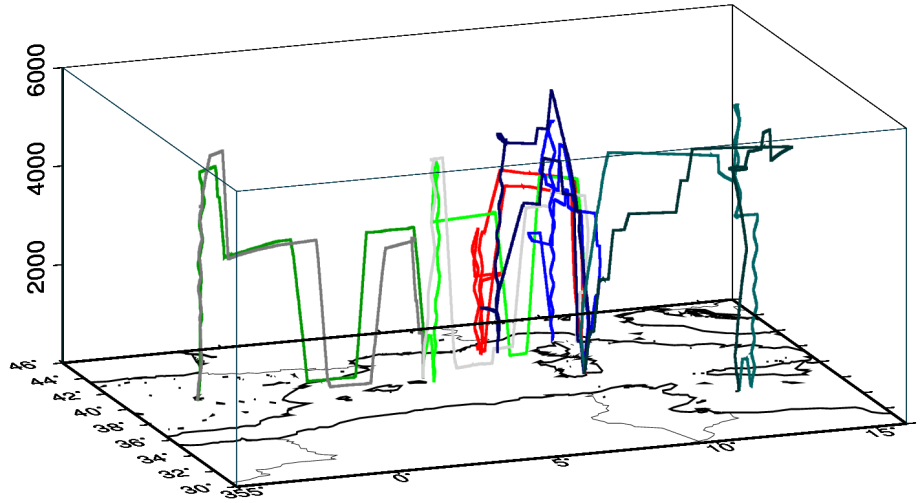

Figure 4. ATR-42 vertical trajectories for the flight of the 14 June (red), 16 and 17 June (blue), 19 and 20 June (green) and 22 June (green-blue).

ACPD
15, 3063–3125, 2015

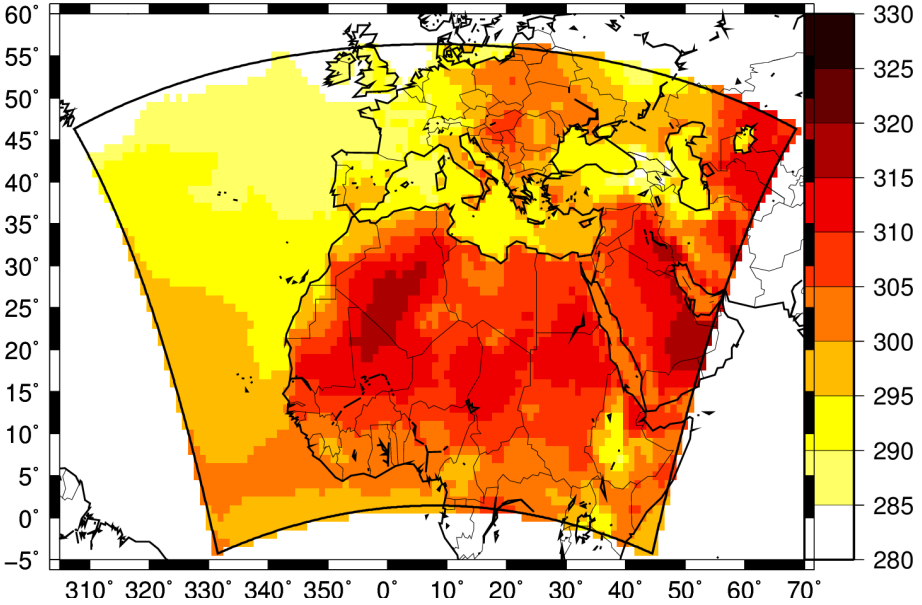

Figure 5. The simulation domain for WRF and CHIMERE. A Lambert conformal projection is used with a constant horizontal resolution of 60 km × 60 km. Colors represent the 2 m temperature (in Kelvin) for the 21 12 June:00 UTC, and the vectors represent the 10 m wind speed.

ACPD
15, 3063–3125, 2015

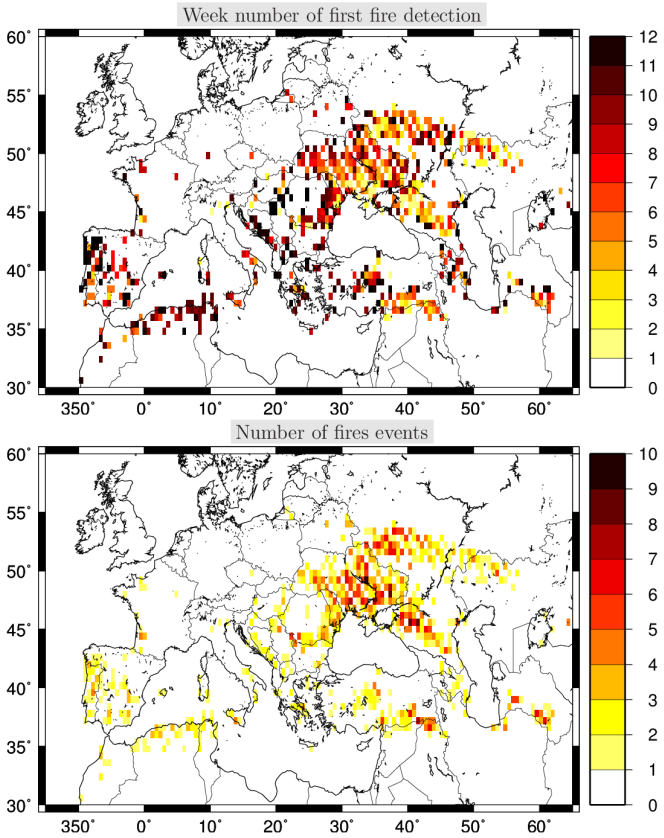

Figure 6. Synthesis of vegetation fires events observed during the summer of 2013, from the 1 June to the 31 August. [top] week of first detection, [bottom] number of events.

ACPD
15, 3063–3125, 2015

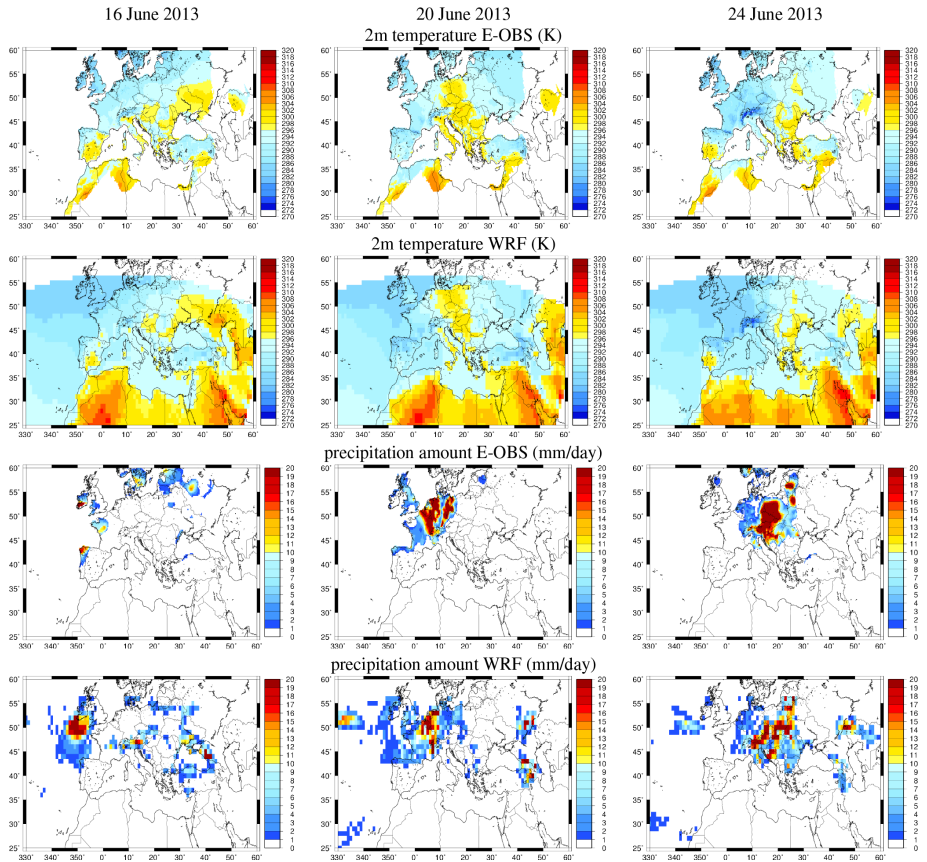

Figure 7. Comparison of daily mean averaged 2 m temperature (K) and daily accumulated precipitation amount (mm day^{-1}) with E-OBS (available over land only) and the WRF meteorological model.

ACPD
15, 3063–3125, 2015

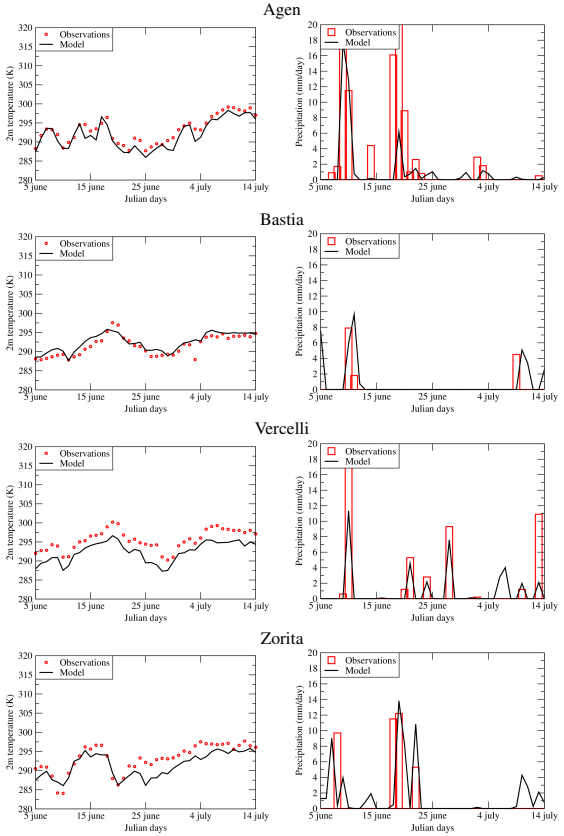

Figure 8. Time series of daily mean averaged 2 m temperature (K) and daily precipitation amount (mm day^{-1}) for several sites where chemical measurements are also available. Time series are extracted from maps of E-OBS daily data.

ACPD
15, 3063–3125, 2015

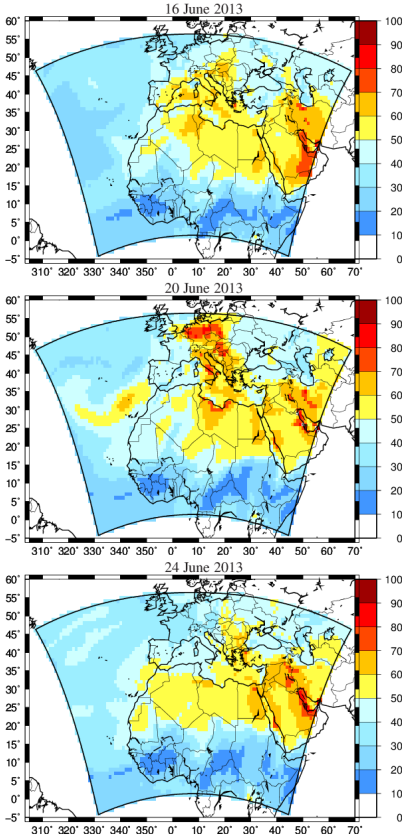

Figure 9. Modelled surface ozone concentrations (µg m^{-3}) for the 16, 20 and 24 June 2013 at 12:00 UTC.

ACPD
15, 3063–3125, 2015

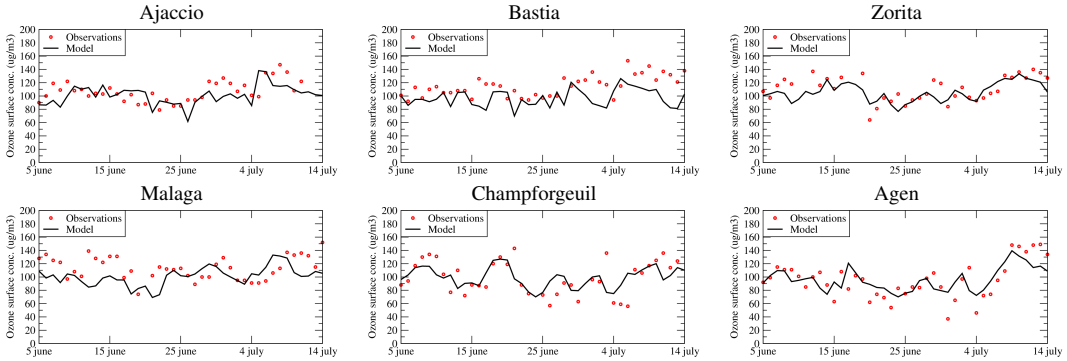

Figure 10. Time series of daily maximum of O_3 surface concentrations for some selected Air-Base sites, continental and coastal stations.

ACPD
15, 3063–3125, 2015

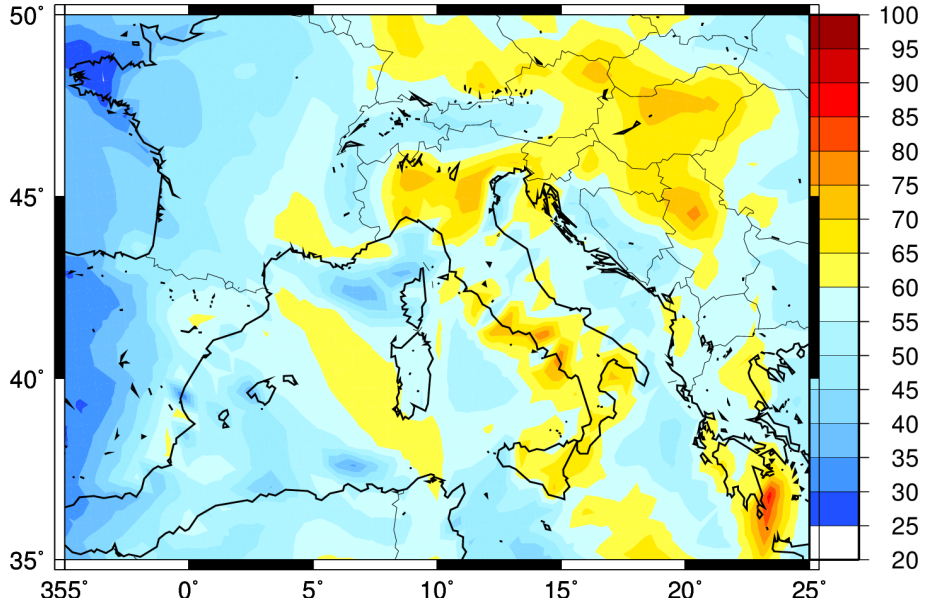

Figure 11. Surface ozone concentrations (ppb) map for the 17 June 2013, 12:00 UTC.

ACPD
15, 3063–3125, 2015

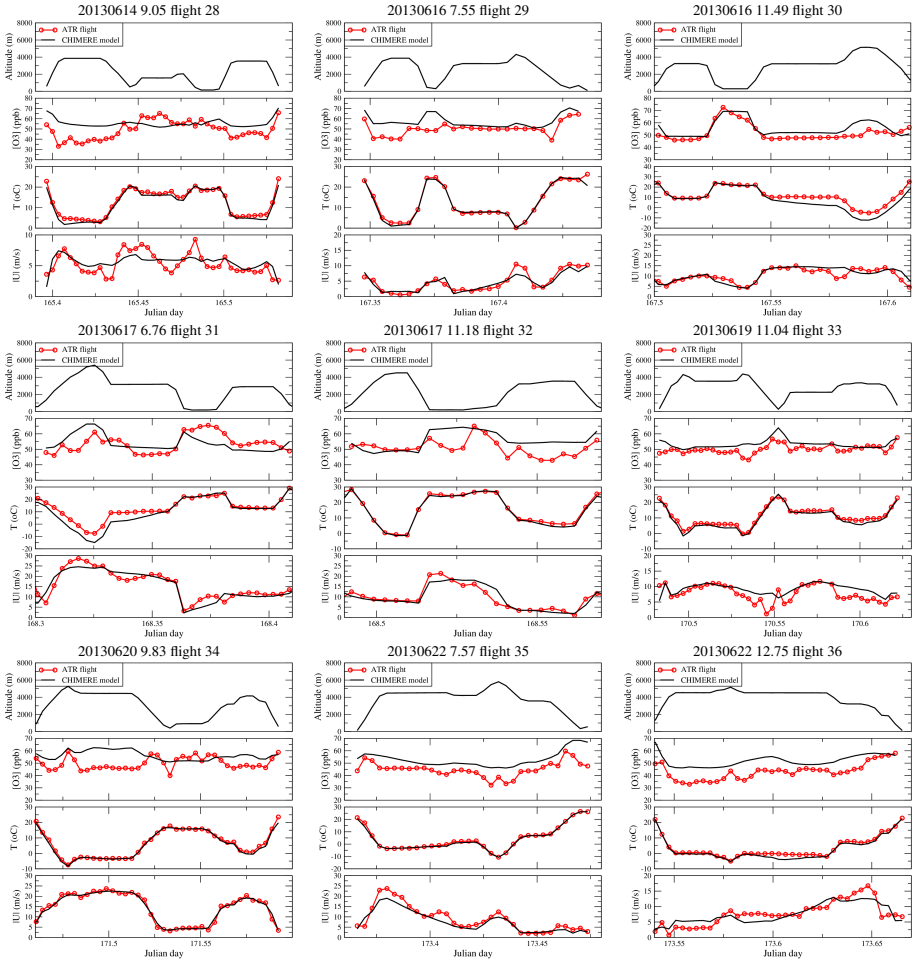

Figure 12. Comparisons between observed and modelled O_3 concentrations, temperature and wind speed along the flight trajectories. The top plot indicates the altitude a.s.l. of the flight.

ACPD
15, 3063–3125, 2015

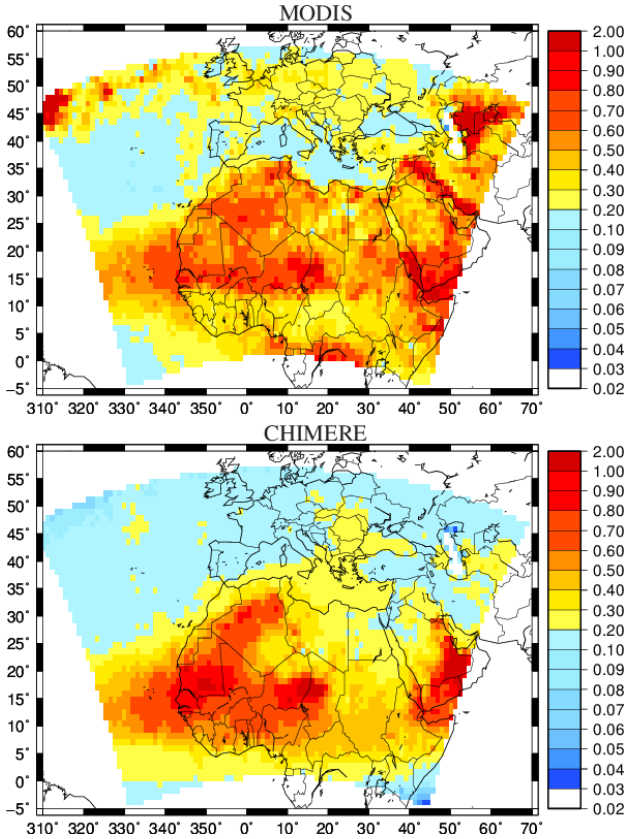

Figure 13. Comparison of Aerosol Optical Depth measured by MODIS (top) and modelled with CHIMERE (bottom). This AOD corresponds to the mean averaged value over the period from 6 June to 15 July 2013.

ACPD
15, 3063–3125, 2015

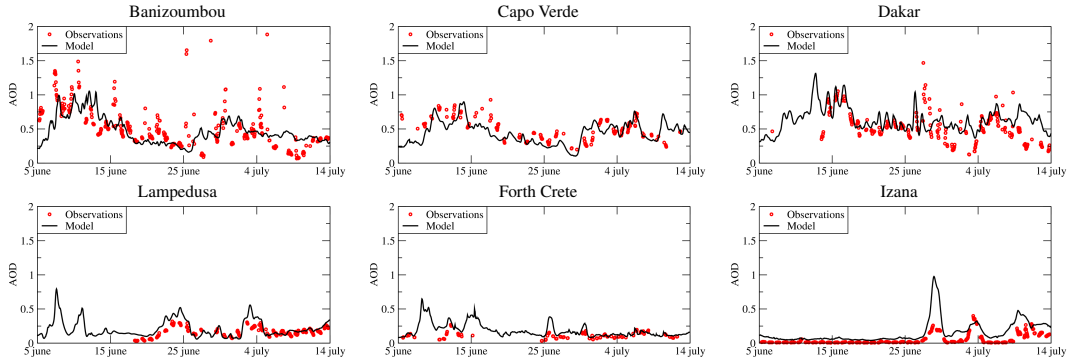

Figure 14. Time series of hourly Aerosol Optical Depth (AOD) for selected AERONET stations.

ACPD
15, 3063–3125, 2015

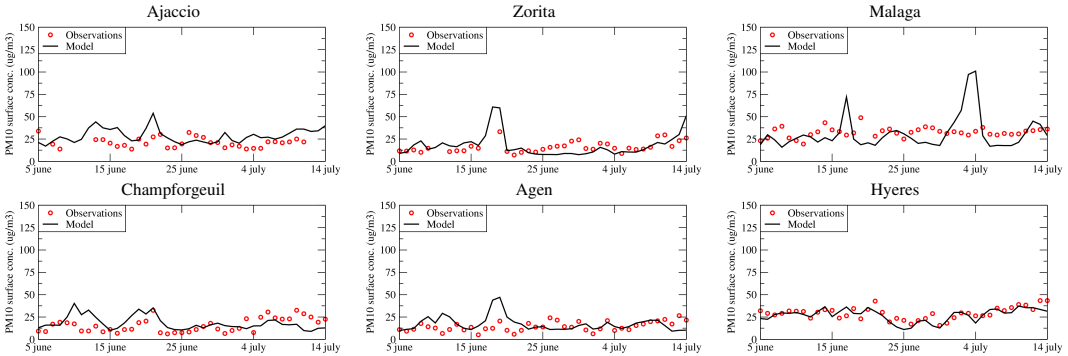

Figure 15. Time series of daily averaged PM_{10} surface concentrations for some selected AirBase sites, continental and coastal stations.

ACPD
15, 3063–3125, 2015

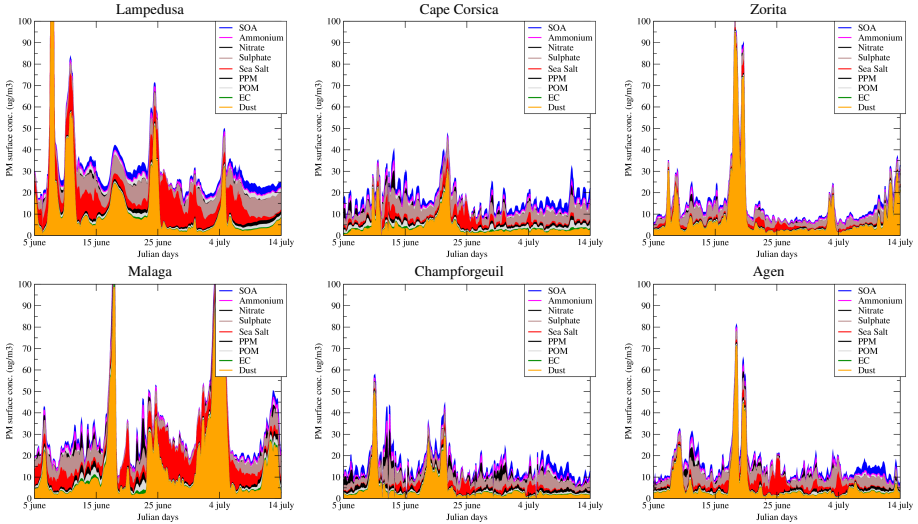

Figure 16. Time series of hourly surface concentrations of all modelled aerosols for the ADRIMED sites (Lampedusa and Cape Corsica) and some selected AirBase sites, continental and coastal stations.

ACPD
15, 3063–3125, 2015

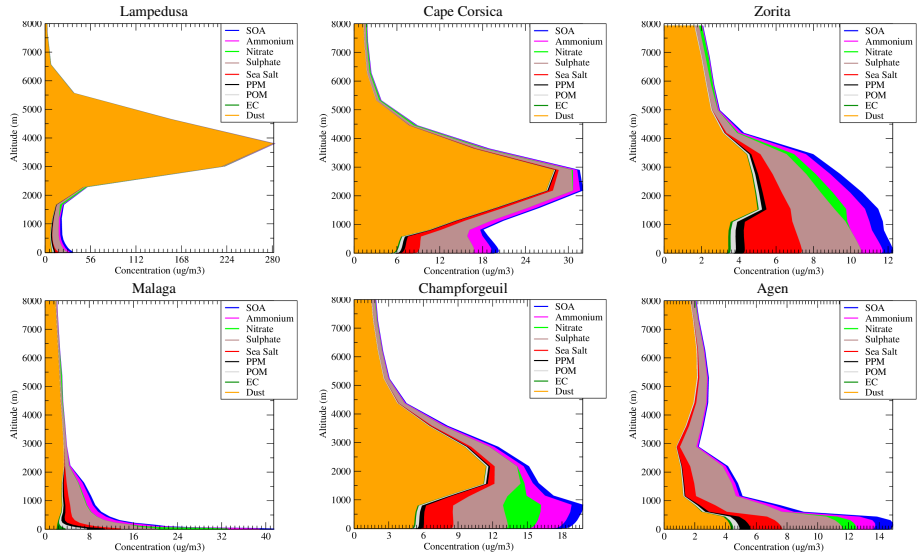

Figure 17. Vertical profiles of all modelled aerosols for the 21 June 2013. Results are presented for the ADRIMED sites (Lampedusa and Cape Corsica) and some selected AirBase sites, continental and coastal stations. Note that the abscissa is different in each plot to better see the values.

ACPD
15, 3063–3125, 2015

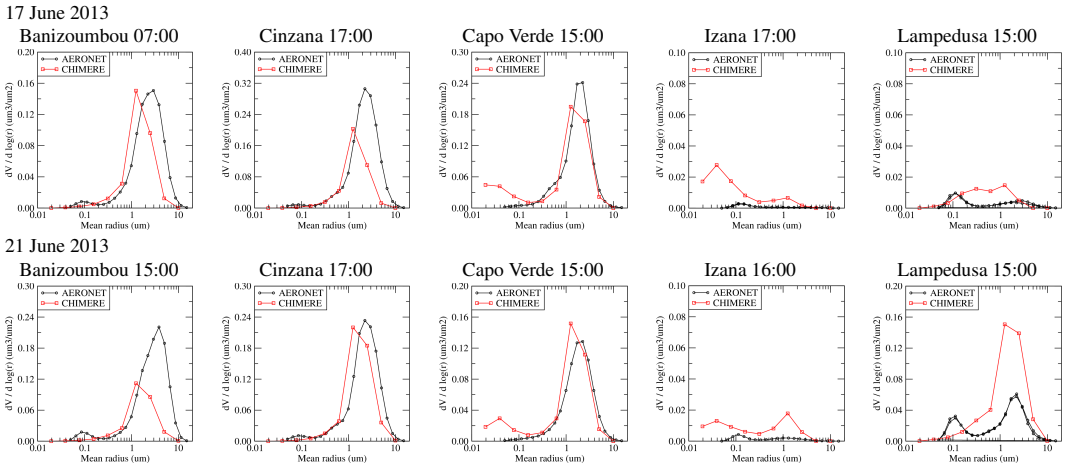

Figure 18. Comparisons between the measured (AERONET) and modelled (CHIMERE) aerosols size distribution for the locations of Banizoumbou, Cinzana, Capo Verde, Izana and Lampedusa. Distributions are presented for the 17 and 21 June 2013, and for hours where the AERONET hourly inverted distributions are available.

ACPD
15, 3063–3125, 2015